N-thiadiazole-4-hydroxy-2-quinolone-3-carboxamides bearing heteroaromatic rings as novel antibacterial agents: Design, synthesis, biological evaluation and target identification

Wenjie Xue, Xueyao Li, Guixing Ma, Hongmin Zhang, Ya Chen, Johannes Kirchmair, Jie Xia, Song Wu

PII: S0223-5234(19)31180-8

DOI: https://doi.org/10.1016/j.ejmech.2019.112022

Reference: EJMECH 112022

To appear in: *European Journal of Medicinal Chemistry*

Received Date: 28 August 2019

Revised Date: 22 December 2019

Accepted Date: 29 December 2019

Please cite this article as: W. Xue, X. Li, G. Ma, H. Zhang, Y. Chen, J. Kirchmair, J. Xia, S. Wu, *N*-thiadiazole-4-hydroxy-2-quinolone-3-carboxamides bearing heteroaromatic rings as novel antibacterial agents: Design, synthesis, biological evaluation and target identification, *European Journal of Medicinal Chemistry* (2020), doi: https://doi.org/10.1016/j.ejmech.2019.112022.

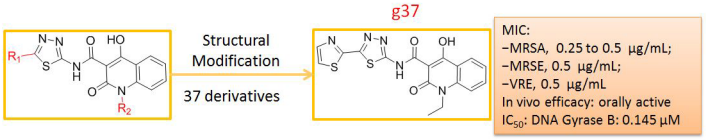

N-Thiadiazole-4-Hydroxy-2-Quinolone-3-Carboxamides Bearing Heteroaromatic Rings as Novel Antibacterial Agents: Design, Synthesis, Biological Evaluation and Target Identification

Wenjie Xue[a], Xueyao Li[a], Guixing Ma[b], Hongmin Zhang[b], Ya Chen[c], Johannes Kirchmair[c,d,e], Jie Xia[a,*] and Song Wu[a,*]

[a] *State Key Laboratory of Bioactive Substance and Function of Natural Medicines, Department of New Drug Research and Development, Institute of Materia Medica, Chinese Academy of Medical Sciences and Peking Union Medical College, Beijing 100050, China;* [b] *Department of Biology, Guangdong Provincial Key Laboratory of Cell Microenvironment and Disease Research, Shenzhen Key Laboratory of Cell Microenvironment and SUSTech-HKU Joint Laboratories for Matrix Biology, Southern University of Science and Technology, Shenzhen 518055, China;* [c] *Center for Bioinformatics (ZBH), Department of Computer Science, Faculty of Mathematics, Informatics and Natural Sciences, Universität Hamburg, Hamburg, Germany. ;* [d] *Department of Chemistry, Faculty of Mathematics and Natural Sciences, University of Bergen, Bergen, Norway;* [e] *Computational Biology Unit (CBU), University of Bergen, Bergen, Norway.*

[*]Correspondence should be addressed to J.X. (jie.william.xia@hotmail.com) or S.W. (ws@imm.ac.cn)

Dr. Jie Xia & Prof. Song Wu

Institute of Materia Medica, Chinese Academy of Medical Sciences

No. 2 Nanwei Road

Beijing 100050, China

Abstract

Due to the occurrence of antibiotic resistance, bacterial infectious diseases have become a serious threat to public health. To overcome antibiotic resistance, novel antibiotics are urgently needed. N-thiadiazole-4-hydroxy-2-quinolone-3-carboxamides are a potential new class of antibacterial agents, as one of its derivatives was identified as an antibacterial agent against *S. aureus*. However, no potency-directed structural optimization has been performed. In this study, we designed and synthesized 37 derivatives, and evaluated their antibacterial activity against *S. aureus* ATCC29213, which led to the identification of ten potent antibacterial agents with minimum inhibitory concentration (MIC) values below 1 μg/mL. Next, we performed bacterial growth inhibition assays against a panel of drug-resistant clinical isolates, including methicillin-resistant *S. aureus*, and cytotoxicity assays with HepG2 and HUVEC cells. One of the tested compounds named 1-ethyl-4-hydroxy-2-oxo-N-(5-(thiazol-2-yl)-1,3,4-thiadiazol-2-yl)-1,2-dihydroquinoline-3-carboxamide (**g37**) showed 2 to 128-times improvement compared with vancomycin in term of antibacterial potency against the tested strains (MICs: 0.25 to 1 μg/mL vs. 1 to 64 μg/mL) and an optimal selective toxicity (HepG2/MRSA, 110.6 to 221.2; HUVEC/MRSA, 77.6-155.2). Further, comprehensive evaluation indicated that **g37** did not induce resistance development of MRSA over 20 passages, and it has been confirmed as a bactericidal, metabolically stable, orally active antibacterial agent. More importantly, we have identified the *S. aureus* DNA gyrase B as its potential target and proposed a potential binding mode by molecular docking. Taken together, the present work reports the most potent derivative

of this chemical series (**g37)** and uncovers its potential target, which lays a solid foundation for further lead optimization facilitated by the structure-based drug design technique.

Keywords: antibiotic resistance, antibacterial agent, MRSA, DNA gyrase B, molecular docking

1. Introduction

Antibiotic resistance has been declared a serious threat to public health worldwide in 2001 and is still on the rise [1]. The bacteria resistant to most antibiotics in clinical use are mainly ESKAPE species, i.e. *E. faecium, S. aureus, K. pneumoniae, A. baumannii, P. aeruginosa* and *Enterobacter* [2, 3]. Among them, the Gram-positive bacteria represented by methicillin-resistant *S. aureus* (MRSA) and vancomycin-resistant *E. faecium* (VRE) have been categorized as serious threats by the US Centers for Disease Control and Prevention in 2013 [4]. The situation becomes even worse as the number of new drugs approved for the treatment of drug-resistant bacterial infections is on the decline in recent years [5, 6]. For these reasons, the discovery of novel resistance-breaking antibacterial agents is of utmost importance.

N-thiadiazole-4-hydroxy-2-quinolone-3-carboxamides represent an important chemical series that shows a wide range of pharmacological activities. Several derivatives have been reported as anticancer agents [7], fat storage regulators [8], strand transfer inhibitors of HIV integrase [9] and anti-tuberculosis agents [10-12]. Compound **11** is a derivative with a methyl group at the position 1 of the 1,2-dihydroquinoline and an ethyl group at the position 5 of the thiadiazol (cf. Figure 1). Peternel L. *et al*. have discovered that this compound is able to inhibit *S. aureus* ATCC 25923 and not toxic to the ChoK1 cell line, with a TC_{50}/MIC ratio of 20.7 [13]. To the best of our knowledge, current pipelines for antibiotics research and development do not cover this chemical series. In addition, no structural modification that improves the potency of compound **11** against *S. aureus* or other gram-positive bacteria has been reported. Although the other reported derivatives

might be repurposed for antibiotics against gram-positive bacteria, they are limited to the structures with alkyl groups at the above-mentioned positions.

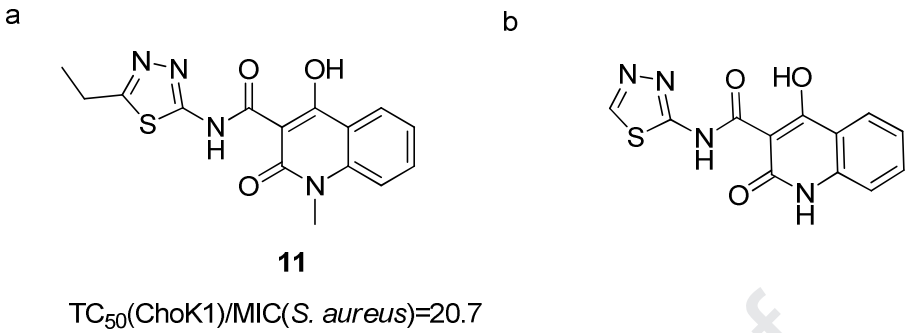

Figure. 1. (a) Antibacterial compound **11** with a desired safety margin and (b) its core scaffold, i.e., N-thiadiazole-4-hydroxy-2-quinolone-3-carboxamide.

In order to develop N-thiadiazole-4-hydroxy-2-quinolone-3-carboxamides as a new class of antibacterial agents, we herein performed structural modification of compound **11 (**mainly with aromatic or heteroaromatic rings at the position 5 of the thiadiazol) and determined the MICs (minimum inhibitory concentrations) of 37 new derivatives against *S. aureus* ATCC 29213. Then, we tested the derivatives that showed higher potencies than compound **11** for their antibacterial activity spectrum and cytotoxicity to HepG2 and HUVEC cells and selected the most promising derivative. Moreover, we evaluated it for its propensity to develop bacterial resistance, its mode of action (i.e. bactericidal or bacteriostatic), *in vitro* metabolic stability, *in vivo* pharmacokinetic profile and *in vivo* antibacterial efficacy. Lastly, we identified its potential target by cheminformatics analysis and proposed a binding mode by molecular docking, which can make structure-based lead optimization become feasible in the future.

2. Results and discussions

2.1. Molecular design

It should be noted that structural modification with the aim to improve the antibacterial potency of the compound **11** has never been reported up to now. As a pioneering work, we designed 37 new structures (cf. Table 1) iteratively by taking into account bioassay results and the commercial availability of the starting materials. At first, we designed three derivatives with alkyl groups, i.e. the methyl, ethyl and propyl groups at position 1 of the 1,2-dihydroquinoline, while leaving position 5 of the thiadiazol unsubstituted. Once the optimal alkyl group was determined, we designed four classes of compounds with different substituents at position 5 of the thiadiazol. Since this position of compound **11** was substituted with an ethyl group, it was natural to design derivatives with alkyl groups in various carbon-atom lengths. Thus, we designed the first class of derivatives that were substituted with methyl, ethyl, *n*-propyl, *n*-butyl, *n*-pentyl and *n*-hexyl groups. As cycloalkyl groups may show similar properties to the alkyl groups, we introduced three cycloalkyl groups (cyclopropyl, cyclopentyl and cyclohexyl groups) to the position, which constituted the second class of derivatives. In order to enhance structural novelty, we further designed the other two classes of derivatives by respectively introducing aromatic rings (benzene rings unsubstituted and those substituted with fluoro, chloro, bromo, difluoromethoxy, nitro, methyl, methoxy, ethoxyl and dimethylamino groups at the *ortho*-, *meta*- or *para*- positions), and heteroaromatic rings (pyridin-2-yl, pyridin-3-yl, pyridin-4-yl, thiophen-2-yl, 1-methyl-1H-pyrazol-3-yl, thiazol-4-yl, thiazol-2-yl groups) to position 5 of the thiadiazol.

2.2. Chemistry

The designed molecules, i.e. *N*-thiadiazol-4-hydroxy-2-quinolone-3-carboxamides, were synthesized according to the route described in Scheme 1, which included the reactions between the 4-hydroxy-2-oxo-1,2-dihydroquinoline-3-carboxylic acids (**c1-c3**) and the substituted aminothiadiazoles (**f1-f35**).

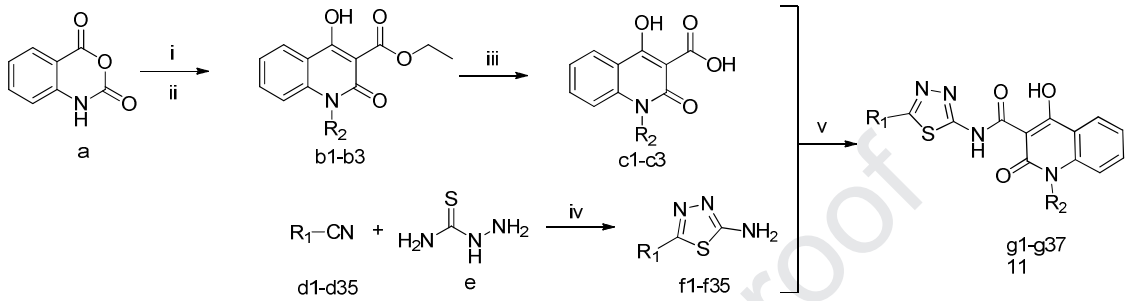

Scheme 1. Reagents and conditions: (i) NaH, 0 °C, DMF, R_2-X (X=I), (ii) NaH, DMF, diethyl malonate, (iii) 2.8 M HCl in CH_3COOH, 60 °C, (iv) TFA, 80 °C, 8 h, (v) EDCI, HOBt, DIPEA, DMF, r.t..

The synthesis of the 4-hydroxy-2-oxo-1,2-dihydroquinoline-3-carboxylic acids (**c1-c3**) started with the isatoic anhydrides (**a**). Firstly, the isatoic anhydrides were alkylated in the presence of both sodium hydride and the alkyl iodide. The resulting *N*-alkylated anhydrides were treated with diethyl malonate and sodium hydride to yield the *N*-alkylated 4-hydroxy-2-oxo-1,2-dihydroquinoline-3-carboxylates (**b1-b3**). These esters were then transformed into the acids by the hydrolysis reaction in a solution of hydrochloric acid dissolved in acetic acid. The 2-amino-1,3,4-thiadiazoles (**f1-f35)** were prepared by the reactions between the nitriles (**d1-d35)** and the thiosemicarbazide (**e**) dissolved in trifluroacetic acid (TFA) [14]. The end products (**11** and **g1-g37**) were obtained by the cross-linking reactions between the 4-hydroxy-2-oxo-1,2-dihydroquinoline-3-carboxylic acids (**c1-c3**) and the 2-amino-1,3,4-thiadiazoles (**f1-f35**). The chemical structures were

validated by high resolution mass spectrometry (HRMS), ^{1}H NMR and ^{13}C NMR (cf. Figure S1).

2.3. Preliminary structure-antibacterial activity relationship

We tested all the synthesized derivatives for their antibacterial activity (i.e. MICs) against *S. aureus* ATCC29213 (i.e. a wild-type and methicillin-sensitive standard strain) by the broth microdilution method. The chemical structures of 37 derivatives (**11** and **g1-g37**) and their MIC values for *S. aureus* ATCC 29213 are listed in Table 1. The MIC values range from 100 μg/mL to 0.1 μg/mL, indicating that all the derivatives inhibit the growth of *S. aureus* ATCC 29213. Encouragingly, ten out of the 37 newly designed and synthesized derivatives **(g1-g37)** were more potent than compound **11** (MIC: 1.56 μg/mL), with MIC values lower than 1 μg/mL. The MIC values of five derivatives even reached up to 0.1 μg/mL. The data demonstrate that our strategy for molecular design was effective to improve antibacterial potency.

As we mention in the subsection of "Molecular design", we initially designed, synthesized and tested three derivatives with different alkyl groups at position 1 of the 1,2-dihydroquinoline (**g1-g3**). As compound **g2** with the ethyl group was more potent than the others (MIC: 1.56 μg/mL; cf. Table 1), we decided to preserve the ethyl group at position 1 of the 1,2-dihydroquinoline when performing further modification at position 5 of the thiadiazol.

Among other derivatives with the ethyl group at R_2, the first class covered those with alkyl groups as R_1. With the exception of **g9**, all compounds of this class (**g4-g9**) exhibited strong antibacterial activity, with MIC values lower than 1 μg/mL. The MIC values were

0.78 μg/mL for the derivatives with the methyl group (**g4**) or the ethyl group (**g5**), 0.39 μg/mL for the derivatives with the *n*-propyl- group (**g6**) and 0.1 μg/mL for the derivatives with the *n*-butyl- (**g7**) or the *n*-pentyl (**g8**) group, respectively (cf. Table 1). For this class of derivatives, it was concluded that (i) the introduction of the alkyl groups in a length within five carbon atoms to the 5-position of the thiadiazol was favorable for antibacterial activity, (ii) the length of the alkyl groups affected the antibacterial activity, and four or five carbon-atom length led to the optimal potency.

The second class of derivatives were those with the cycloalkyl substituents, including **g10** (the cyclopropyl group), **g11** (the cyclopentyl group) and **g12** (the cyclohexyl group). Their MIC values were greater than that of **g2**, indicating that the introduction of the cycloalkyl groups results in a decrease of antibacterial activity.

The third class of derivatives started with **g13**, i.e. the derivative with the benzene ring. Compound **g13** was as potent as the compounds bearing alkyl groups (MIC: 0.39 μg/mL; cf. Table 1). This outcome was rather encouraging because no aromatic ring had been reported as a substituent at position 5 of the thiadiazol for N-thiadiazole-4-hydroxy-2-quinolone-3-carboxamides so far. As a follow-up, we designed and synthesized 17 derivatives with a variety of substituted benzene rings (**g14-g30)** through parallel synthesis. The bioassay data suggested a preliminary structure-activity relationship (SAR) for this class of derivatives: (i) All the substitutions in the benzene ring reduced the antibacterial activity. The introduction of the electron-withdrawing groups seemed to be more detrimental to antibacterial activity than the electron-donating groups (e.g. the methoxy group). For instance, the derivative with the fluoro- group at the *ortho*-,

meta- or *para*- position was not as potent as that with the methoxy group at the same position. As shown in Table 1, **g27** (MIC: 12.5 μg/mL), **g23** (MIC: 6.25 μg/mL) and **g14** (MIC: 25 μg/mL) are less potent than **g29** (MIC: 3.12 μg/mL), **g25** (MIC: 1.56 μg/mL) and **g20** (MIC: 3.12 μg/mL), respectively. (ii) Whether the substituent of the benzene ring was an electron-donating group or an electron-withdrawing group, the *meta*- position for substitution seemed to be better than the other two positions. For instance, the derivatives with the fluoro, the methoxy or the ethoxyl group at the *meta*- position (i.e. **g23**, **g25**, **g26**) showed better antibacterial activity than those with the substituents at the *ortho*- and the *para*- positions (i.e. **g27**/**g14**, **g29**/**g20**, **g30**/**g21**).

Seven derivatives with different heteroaromatic rings (**g31**-**g37**) belong to the fourth class of derivatives. Among them, **g31** (the pyridin-2-yl group**)** and **g37** (the thiazol-2-yl group**)** showed four-fold improvement in antibacterial activity compared with **g13** (phenyl group), with a MIC value as low as 0.1 μg/mL. The compounds **g32** and **g36** were also potent antibacterial compounds (MIC: less than 1 μg/mL). To be specific, **g32 (**pyridin-3-yl group) displayed the activity equivalent to **g13** (MIC: 0.39 μg/mL), while **g36** (thiazol-4-yl group) was slightly weaker (MIC: 0.78 μg/mL) than **g13**.

Table 1. Chemical structures of the synthesized compounds, their antibacterial activity in terms of MICs (μg/mL) for *S. aureus* ATCC29213 and GyrB inhibitory activity in term of IC_{50} (μM).

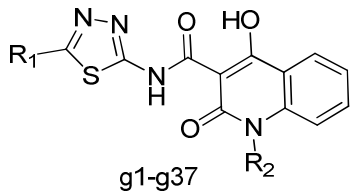

g1-g37

Compound	R_1	R_2	*S. aureus*	IC_{50} for GyrB

ID			ATCC29213	(μM, mean ± SD)[a]
11		CH_3-	1.56	0.10±0.01
g1	H	CH_3-	6.25	0.19±0.03
g2	H	CH_3CH_2-	1.56	0.11±0.01
g3	H	$CH_3(CH_2)_2$-	3.12	0.46±0.03
g4		CH_3CH_2-	0.78	0.24±0.01
g5		CH_3CH_2-	0.78	0.45±0.01
g6	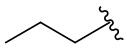	CH_3CH_2-	0.39	0.27±0.01
g7	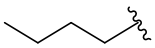	CH_3CH_2-	0.1	0.99±0.01
g8	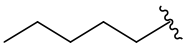	CH_3CH_2-	0.1	0.47±0.02
g9	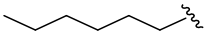	CH_3CH_2-	12.5	0.35±0.02
g10		CH_3CH_2-	3.12	0.58±0.10
g11	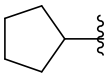	CH_3CH_2-	6.25	0.55±0.01
g12	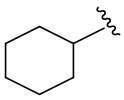	CH_3CH_2-	12.5	0.55±0.06
g13	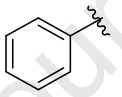	CH_3CH_2-	0.39	1.72±0.10
g14	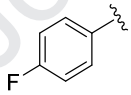	CH_3CH_2-	25	2.30±0.04
g15	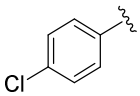	CH_3CH_2-	12.5	1.46±0.20
g16	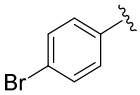	CH_3CH_2-	12.5	2.19±0.24
g17	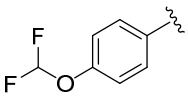	CH_3CH_2-	12.5	1.42±0.02
g18	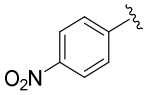	CH_3CH_2-	50	1.61±0.16

g19	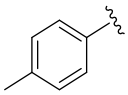	CH_3CH_2-	6.25	0.64±0.07
g20	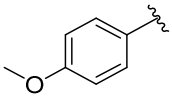	CH_3CH_2-	3.12	1.14±0.14
g21	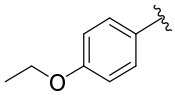	CH_3CH_2-	100	2.30±0.11
g22	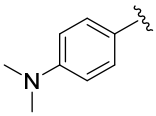	CH_3CH_2-	3.12	2.66±0.13
g23	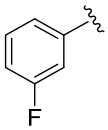	CH_3CH_2-	6.25	1.81±0.25
g24	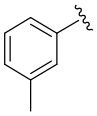	CH_3CH_2-	12.5	1.75±0.03
g25	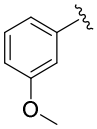	CH_3CH_2-	1.56	2.17±0.05
g26	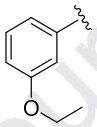	CH_3CH_2-	3.12	1.69±0.06
g27	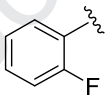	CH_3CH_2-	12.5	0.99±0.16
g28	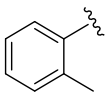	CH_3CH_2-	50	3.18±0.11
g29	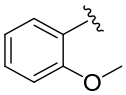	CH_3CH_2-	3.12	0.76±0.01
g30	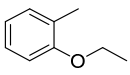	CH_3CH_2-	12.5	2.35±0.08
g31		CH_3CH_2-	0.1	0.42±0.05
g32		CH_3CH_2-	0.39	0.24±0.02

g33	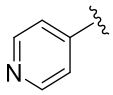	CH_3CH_2-	1.56	0.24±0.03
g34	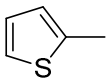	CH_3CH_2-	3.12	0.22±0.05
g35	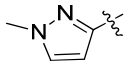	CH_3CH_2-	3.12	0.49±0.04
g36	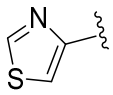	CH_3CH_2-	0.78	0.16±0.03
g37	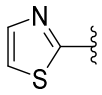	CH_3CH_2-	0.1	0.15±0.02

[a] mean, the average of the duplicate; SD, standard deviation.

2.4. Activity spectrum against a panel of gram-positive bacteria

Following the discovery of ten compounds that potently inhibited methicillin-sensitive *S. aureus* (MSSA) ATCC 29213 (MIC: less than 1 μg/mL), we tested them against other nine strains of MRSA, including clinical isolates (15-1, 15-2, 15-3, 15-6, 15-7, 15-8, 15-9, ATCC 700699 and ATCC 700788), with compound **11** as a reference and vancomycin as a positive control. Compared with their potency for MSSA (0.1 to 0.78 μg/mL), all new derivatives showed decreased potency for the tested MRSA strains, with MIC values ranging from 0.25 μg/mL to >64 μg/mL (cf. Table 2). Among them, the MIC values of the derivatives with the aromatic rings except for **g36** ranged from 0.25 to 2 μg/mL, while the MIC values of those with the alkyl groups except for **g8** were between 0.5 to >64 μg/mL. The above data indicate that the introduction of the aromatic rings at position 5 of the thiadiazol is more favorable for antibacterial activity against MRSA strains than the substitutions with the alkyl groups. This observed structure-activity relationship was further validated by the bioassay against other Gram-positive bacteria, including methicillin-sensitive *S. epidermidis* (MSSE), methicillin-resistant *S. epidermidis* (MRSE),

E. faecalis (EFA), E. faecium (EFM) and vancomycin-resistant *E. faecalis* (VRE). For these bacteria, the MIC values of most derivatives with aromatic rings (**g13**, **g31** and **g37)** are lower than those with alkyl groups (**g4-g7)**.

Among derivatives with alkyl groups (including compound **11**), the most potent compound was **g8**. Its MIC values for the tested bacterial strains were between 0.5 and 2.0 μg/mL and hence lower than those of vancomycin (MICs: 1.0 to 64.0 μg/mL). Importantly, **g8** remained active against VRE and two vancomycin-intermediate *S. aureus* (VISA) strains, i.e. ATCC700699b and ATCC700788b. Among those derivatives with the aromatic rings, **g31** and **g37** were the only two compounds that showed better antibacterial activity than vancomycin for most of the tested bacterial strains. **g37** seemed to be a bit more potent (MICs: 0.25-1 μg/mL) than **g31 (**MICs: 0.5-1 μg/mL**)**. In particular, **g37** was able to inhibit the growth of the three VRE strains at the concentration of 0.5 μg/mL. while the MIC value of **g31** for these strains was 1 μg/mL.

2.5. Cytotoxicity to HepG2 and HUVEC cells

Since the essence of antibacterial therapy is selective toxicity [13], i.e. to kill or inhibit bacteria while not to harm patients, mammalian cell toxicity is a common metric for antibacterial drug discovery. In this study, we tested **g8** (with alkyl groups), **g31** and **g37** (with the aromatic/heteroaromatic rings) for their cytotoxicity against two cell lines, i.e. human hepatocellular carcinoma (HepG2) cells and human umbilical vein endothelial cells (HUVEC) using the sulforhodamine B (SRB) assay [15]. As shown in Table 3, the IC_{50} values of the three compounds were greater than 50 μg/mL for HepG2 cells and over 25 μg/mL for HUVEC cells. To determine the compound with the highest safety margin, we

calculated the selectivity indexes (SIs) for the three compounds by considering both the IC_{50} and MIC values for the MRSA strains. The SI values of **g37** for both HepG2 and HUVEC were 110.6 to 221.2 and 77.6 to 155.2, respectively, and hence greater than those of **g8** and **g31** (HepG2: 52.1 to 104.2 and 63.2 to 126.4; HUVEC: 41.9 to 83.8 and 26.5 to 53). According to the safety margins, we selected **g37** for further bioassay.

2.6. Comprehensive evaluation of g37

2.6.1. Propensity to develop bacterial resistance

In order to study the propensity of bacterial strains to develop resistance to **g37**, we treated the bacterial strain MRSA 15-1 with the sub-lethal concentration (0.5×MIC) of **g37** to make it potentially develop resistance. The way to study resistance development had been commonly used in antibacterial drug discovery [16-18]. Then, we determined the MIC value of **g37** against the bacterial strain selected by the compound treatment. The compound treatment and the MIC determination were repeated for 20 passages. Figure 2 and Table S1 show the MIC variability of **g37** during 20 passages of the test, with vancomycin as a comparison. Clearly, the sub-lethal level of vancomycin induced the development of bacterial resistance to vancomycin, as the MIC value increased from 1 μg/mL to 8 μg/mL. Encouragingly, the MIC values of **g37** remained unchanged (0.5 μg/mL) during 20 passages, which indicated that **g37** did not induce the development of drug-resistant bacterial strain.

Table 2. Antibacterial activity spectrum of ten potent derivatives (MIC: less than 1 μg/mL for *S. aureus* ATCC29213) and compound **11**.

Bacterium[a]	Strain	MIC (μg/mL)											
		11	**g4**	**g5**	**g6**	**g7**	**g8**	**g13**	**g31**	**g32**	**g36**	**g37**	Vancomycin
MRSA	15-1	2	2	2	2	2	0.5	2	0.5	0.5	4	0.5	1
	15-2	4	4	2	2	2	1	2	1	0.5	4	0.5	1
	15-3	2	2	2	2	2	0.5	1	0.5	0.5	4	0.5	1
	15-6	4	2	2	2	2	0.5	0.5	0.5	0.5	4	0.5	1
	15-7	4	4	1	4	4	0.5	1	1	0.5	4	0.5	1
	15-8	4	2	1	2	2	0.5	0.5	0.5	0.5	4	0.5	1
	15-9	4	4	1	4	2	1	0.25	1	0.5	4	0.25	1
	ATCC700699[b]	4	>64	2	4	4	1	2	0.5	1	4	0.5	4
	ATCC700788[b]	4	>64	2	4	4	1	2	0.5	1	4	0.5	8
MSSE	15-3	4	>64	2	2	2	1	1	1	2	8	0.5	2
	15-4	2	>64	2	2	2	1	1	1	1	4	0.5	2
MRSE	15-1	4	>64	2	2	2	1	1	1	1	4	0.5	1
	15-2	4	>64	2	4	2	1	1	1	1	8	0.5	2
	15-3	4	>64	2	2	2	1	1	1	1	4	0.5	2
EFA	15-1	4	>64	2	4	2	2	1	1	>64	4	0.5	2
	15-2	4	>64	2	4	2	1	1	1	>64	4	0.5	2
EFM	15-1	4	>64	4	2	2	1	1	1	>64	8	1	1
	15-2	4	>64	2	4	2	1	2	1	>64	4	1	2
VRE	ATCC51299	32	>64	8	8	8	1	1	1	>64	32	0.5	32
	ATCC700802	32	>64	8	8	8	1	1	1	>64	32	0.5	64
	ATCC51575	32	>64	8	8	8	1	1	1	>64	32	0.5	64

[a]: MRSA, methicillin-resistant *S. aureus*; MSSE, methicillin-sensitive *S. epidermidis*; MRSE, methicillin-resistant *S. epidermidis*; EFA, *E. faecalis*; EFM, *E. faecium*; VRE, vancomycin-resistant *E. faecalis*.

[b]: vancomycin intermediate sensitive *S. aureus* (VISA)

Table 3. Cytotoxicity of three compounds to HepG2 and HUVEC cells.

Compound ID	IC_{50} (μM, mean ± SD)[a]		SI[b]	
	HepG2	HUVEC	HepG2	HUVEC
g8	52.1±12.9	41.9±5.4	52.1-104.2	41.9-83.8
g31	63.2±7.5	26.5±6.6	63.2-126.4	26.5-53
g37	55.3±8.4	38.8±1.8	110.6-221.2	77.6-155.2
paclitaxel	0.009±0.0039	0.0013±0.0001	n.d.[c]	n.d.

[a] values represent cytotoxicity after 72-hour treatment with compounds. mean, the average of duplicate values; SD, standard deviation.
[b] selectivity index, IC_{50}/MIC_{MRSAs}
[c] n.d., not determined.

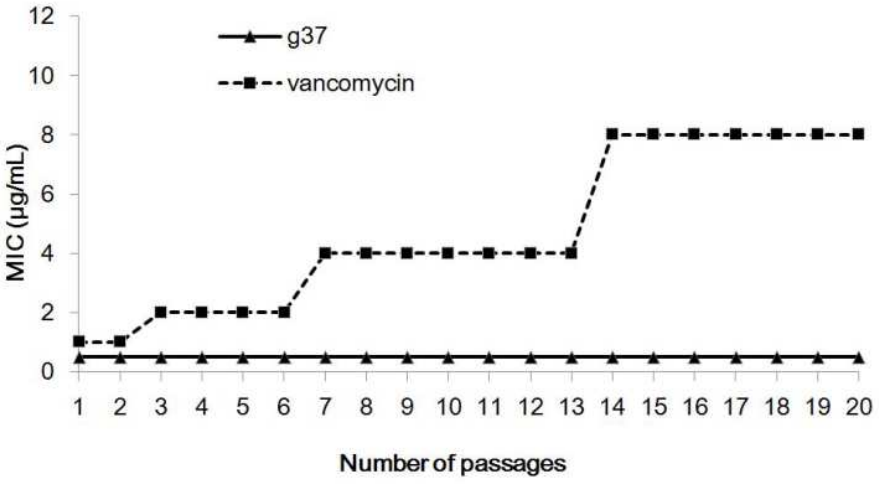

Figure 2. The MIC variability of **g37** (▲) and vancomycin (■) against MRSA 15-1 during 20 passages of the resistance development assay, with vancomycin as a comparison.

2.6.2. Time-kill kinetics analysis

In order to determine whether our lead compound **g37** was bactericidal or bacteriostatic, we studied its time-kill kinetics against MRSA 15-1 at five concentrations, i.e. 0.5×MIC, 1×MIC, 2×MIC, 4×MIC, 8×MIC. As shown in Figure 3, at 4×MIC (2 μg/mL) and 8×MIC (4 μg/mL) concentrations, **g37** reduced the starting $\log_{10}$ CFU/mL (bacteria concentration) by more than 3 log units over 24 h. Therefore, our lead compound **g37** was

bactericidal. As a comparison, we also performed the time-kill kinetics study for vancomycin. The result showed that also vancomycin was bactericidal as the starting bacterial concentration decreased by more than 3 log units after 24 h of treatment with vancomycin at concentrations of 4×MIC (4 μg/mL) and 8×MIC (8 μg/mL). The time-kill curves also showed differences between **g37** and vancomycin. (i) According to the variability of $\log_{10}$ CFU/mL (4×MIC and 8×MIC), **g37** showed a lower bactericidal rate than vancomycin, but it had an equivalent effect to vancomycin on reducing the bacterial concentration after 24 h. (ii) Treated at lower concentrations (1×MIC and 2×MIC), the bacterial $\log_{10}$ CFU/mL was more significantly reduced by **g37**.

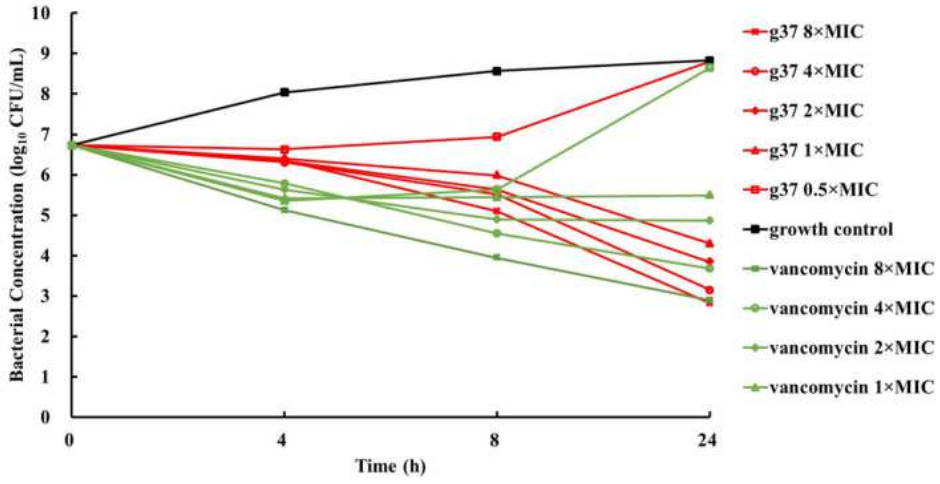

Figure 3. Time-kill kinetics for the compound **g37** and vancomycin against MRSA 15-1 within 24 h. The compound concentrations used in the assays were 0.5×MIC, 1×MIC, 2×MIC, 4×MIC, 8×MIC. Each data point is the average of three measurements.

2.6.3. In vitro metabolic stability and in vivo pharmacokinetic profile

Metabolic stability of small molecules affects in vivo pharmacokinetic profile and thus *in vivo* efficacy. As our systemic infection model was based on mice, we firstly tested the

metabolic stability of **g37** by incubating the compound with the plasma or liver microsomes from mice. As shown in Table 4, the estimated $t_{1/2}$ (i.e. half-life) value in mouse plasma was 503.11 min, indicating **g37** was stable in mouse plasma. Besides, the value of $t_{1/2}$ and CLint (i.e. intrinsic clearance) in liver microsomes was estimated as 35.6 min and 38.9 μL/min/mg proteins, respectively, which indicated **g37** was a compound of slow clearance [19]. Encouraged by the stable *in vitro* metabolism, we then performed a preliminary pharmacokinetic study in mice. The result of the pharmacokinetic study is shown as a curve that describes the concentration viability of **g37** in plasma along with the sampling time after the compound was orally administered at a dose of 10 mg/kg (cf. Figure S3). We obtained the pharmacokinetic parameters from the curve that (1) the maximum concentration (C_{max}) of the compound in plasma (including the free state and the bound state) was 827.1 ng/mL, a concentration a bit greater than its MIC value for the bacterial strain (0.5 μg/mL), (2) the time to reach the maximum concentration (T_{max}) was 1.0 h, (3) the $t_{1/2}$ value of this compound was favorable (2.3 h) and the mean residence time during the sampling time was 2.7 h (cf. Table 4). All the above data demonstrated that **g37** had relatively good pharmacokinetic properties.

Table 4. In vitro metabolic stability and in vivo pharmacokinetics profile of the compound g37.

in vitro metabolic stability (mouse)			mouse pharmacokinetic profile	
	plasma stability	liver microsomes stability	parameter	10mg/kg (p.o.)
$t_{1/2}$ (min)	503.11	35.6	AUC_{last}(h•ng/mL)	2539
			AUC_{inf}(h•ng/mL)	2620
			MRT_{last}(h)	2.7
CLint (μL/min/mg)	/	38.9	$t_{1/2}$ (h)	2.3
			T_{max}(h)	1
			C_{max}(ng/mL)	827.1

2.6.4. In vivo antibacterial efficacy

In light of the favorable biological and pharmacokinetic properties of **g37**, we were curious to see whether the compound would show *in vivo* antibacterial efficacy. Prior to the efficacy study, we determined the minimum lethal dose (MLD) for our Kunming mice as 5 $\times 10^7$ CFU/mL, by the intraperitoneal injection of the MRSA 15-1 inoculum (0.5 mL) at three different doses, i.e. 5×10^7 CFU/mL, 5×10^6 CFU/mL and 5×10^5 CFU/mL (cf. Table S2). As the first attempt, we treated the mouse systematic infection model with the compound according to a common dosing schedule for oral administration of antibiotics, i.e. dosing twice after bacterial infection [20, 21]. Unfortunately, the compound did not protect the mice from death, even at each dose up to 50 mg/kg (cf. Table S3).

Antibiotic prophylaxis, the administration of antibiotics before surgery or a dental procedure, is used in patients who are faced with high risks of bacterial infections [22, 23]. Inspired by this idea, we carried out prophylactic administration at 12 h and 6 h before the injection of the MRSA inoculum. Here, the interval of the prophylactic administration was determined as 6 h, because we would like to keep it consistent with the double-dosing

schedule for the treatment. Then we injected the MRSA inoculum (0.5 mL) at the MLD intraperitoneally to the mice that had been pre-treated by the compound. Subsequently, we orally administered the compound twice, i.e. at 0 h and 6 h post-infection, at the same dose as the prophylactic administration. A significant dose-effect relationship of **g37** was observed from Figure 4a, i.e. a higher dose led to a higher survival rate. All the treated groups demonstrated the improvement in survival rates compared with the vehicle control (i.e. the untreated group, survival rate: 12.5%). The survival rates were 87.5%, 50%, 37.5% and 25%, when treated with the compound at the doses of 9 mg/kg, 3 mg/kg, 1 mg/kg and 0.33 mg/kg, respectively. Linezolid was used as a positive control and administered in the same way as **g37** (including the prophylactic administration). As shown in Figure 4b, both groups of mice treated with linezolid at the doses of 9 mg/kg and 3 mg/kg survived the infection. As a blank control, the uninfected group of mice had a survival rate of 100%. In addition, we treated the uninfected mice with **g37** according to the same dosing schedule (including the prophylactic administration) at each dose as high as 30 mg/kg. Since no death was observed (cf. Table S3), the compound **g37** had a wide therapeutic window.

In order to uncover potential causes of the different effects between the dosing schedules with and without prophylactic administration, we tested mouse plasma protein binding (PPB) of **g37** and found that it was rather high (99.9%). Due to the high PPB, it seems that both pharmacokinetics and pharmacodynamics would be potentially affected by the dosing schedules [24]. Apart from this potential cause, more studies will be performed in the near future to understand the observation.

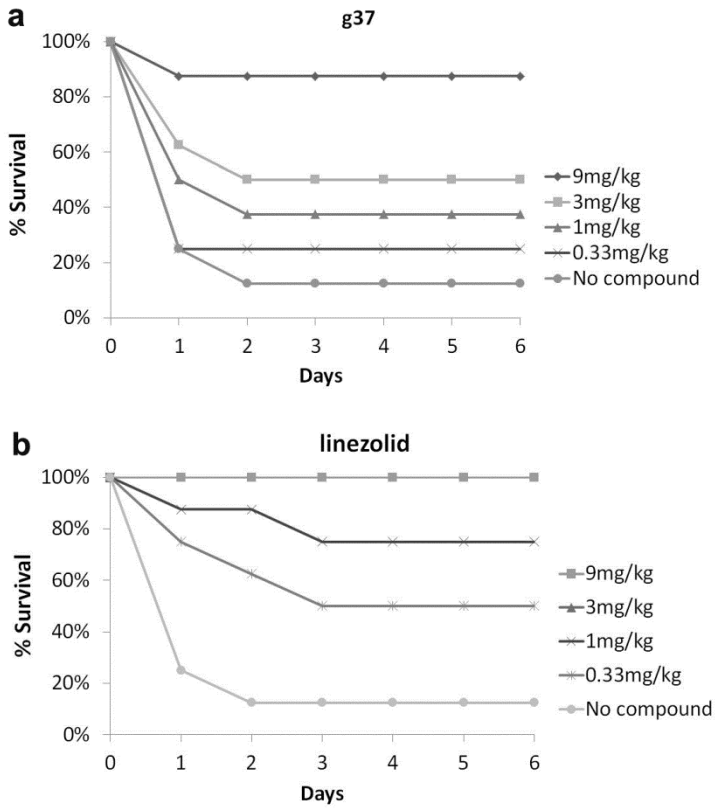

Figure 4. The survival rates of the mice infected with 5×10^7 CFU/mL of MRSA15-1 within 7 days after the treatment of the compound **g37** (**a**) or linezolid (**b**) at four doses ranging from 9 mg/kg to 0.33 mg/kg. The curve for the vehicle control, i.e. the mice that were not treated with the compound is also shown.

2.7. Target Identification

*2.7.1. Inhibition of S. aureus GyrB and DNA supercoiling by **g37***

It was noted that the chemical series studied in this work contained a 2-quinolone scaffold, a bioisostere to coumarins [25]. The natural antibiotic with a coumarin core, i.e. novobiocin, exhibits antibacterial activity by inhibiting the ATPase activity of DNA gyrase B (GyrB) [26]. As the 4-hydroxyl coumarin-3-carbamoyl scaffold of novobiocin is structurally related to the 4-hydroxy-2-oxo-1,2-dihydroquinoline of **g37** (cf. Table S4), we hypothesized that **g37** may inhibit GyrB as well. GyrB, as a subunit of DNA gyrase,

functions to provide energy for DNA supercoiling via catalyzing the hydrolysis of ATP. The ATPase inhibition causes a failure of DNA supercoiling and hence inhibits or kills bacteria [27].

We retrieved all the available GyrB inhibitors (Gram-positive bacteria) from the ChEMBL database 25 (accessed in Apr. 2019)[28, 29] and calculated their structural similarity with **g37**, i.e. Tanimoto coefficients based on MACCS fingerprints. 31 potent GyrB inhibitors (IC_{50}: less than 1 μM) were found to be structurally related to **g37** [30, 31], with Tanimoto coefficients of 0.75 and higher (cf. Table S4). This strengthened the hypothesis that **g37** may target GyrB.

To validate our hypothesis, we measured the production of ADP before and after the treatment of *S. aureus* Gyrase with different concentrations of **g37**. A clear dose-response relationship was observed and the IC_{50} was determined as 0.145 μM (cf. Figure 5a, the IC_{50} of the positive control, i.e. novobiocin, was 0.015 μM, which was consistent with an earlier report [32]). Since GyrB inhibitors eventually impair DNA supercoiling, we tested the effect of **g37** on that process by agarose gel electrophoresis. As shown in Figure 5b, **g37** clearly inhibited the production of the supercoiled DNA in a dose-response manner. The above bioassays confirmed *S. aureus* GyrB as a potential target of **g37**.

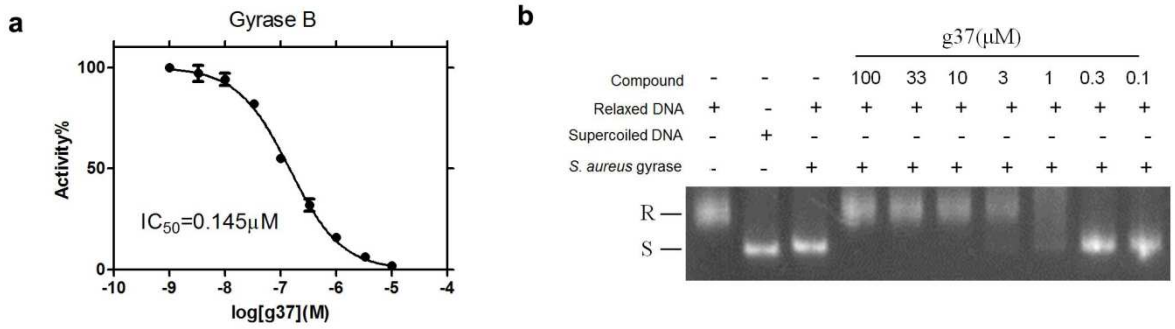

Figure 5. Target validation of **g37**. (a) The concentration-dependent ATPase inhibition of *S. aureus* Gyrase B. The IC_{50} value is 0.145 μM. (b) The effect of the compound **g37** on the DNA supercoiling at serial concentrations, shown by agarose gel electrophoresis. R, the relaxed DNA; S, the supercoiled DNA.

As a follow up, we determined the IC_{50} values of all the other derivatives against *S. aureus* GyrB. As their IC_{50} values were between 0.10 μM and 3.18 μM (cf. Table 1), the whole series of compounds were targeting *S. aureus* GyrB. Apart from that, we noted that (i) all the potent antibacterial compounds (MIC: less than 1 μg/mL) potently inhibited GyrB (IC_{50}: less than 1 μM) as well, with **g13** as the only exception. (ii) For the weak antibacterial compounds (MIC: greater than 1 μg/mL), however, they were not necessarily weak GyrB inhibitors. For instance, the compounds including **g1-g3**, **g9-g12** and **g33-g35** showed moderate antibacterial potency but potent GyrB inhibition. The observations uncovered the potential relationship between enzymatic inhibition and antibacterial activity. To be specific, GyrB inhibition is an important factor for antibacterial activity, but the increase of GyrB inhibition does not ensure strong antibacterial potency.

The homology of GyrB to the E subunit of Topoisomerase IV, i.e. ParE [27] prompted us to measure the effect of **g37** on ParE. As a result, no inhibitory activity was observed (cf.

Figure S3) for **g37**, with the IC_{50} value greater than 100 μM (the IC_{50} value of the positive control, i.e. novobiocin, was 7.9 μM, which was close to an earlier report [32]).

*2.7.2 Potential binding mode of **g37** to S. aureus Gyrase B*

We performed molecular docking to derive a plausible binding mode of **g37** to the ATP binding site of GyrB using the crystal structure of *S. aureus* GyrB bound to novobiocin (PDB code: 4URO). Since Zhang, J. *et al*. highlighted that the cocrystallized water molecule labeled as wat46 was potentially involved in ligand recognition [33], we retained the same water molecule during the docking simulations. Due to the similarity of **g37** and novobiocin in the core scaffold, we hypothesized that the 2-quinolone scaffold may interact with GyrB in the same way as the coumarin core. The most plausible binding pose is shown in Figure 6. Figure 6a shows **g37** and novobiocin share a similar binding mode, in particular the core scaffold, while Figure 6b shows the details of the binding mode. Similar to the coumarin core, the carbanyl group of the 2-quinolone scaffold forms hydrogen bonds with Arg144. In addition, the 2-quinolone scaffold interacts with GyrB via electrostatic interactions with Arg84 and hydrophobic interaction with Pro87. Apart from the similar interactions, **g37** also binds to GyrB through a few unique interactions. To be specific, (i) the thiadiazole may interact with Asp81, Thr173 and Gly85 via the conserved water molecule. Also, it forms the hydrophobic interaction with Ile86 and the electrostatic interaction with Glu58. (ii) The thiazol-2-yl group at the terminus is located at a small and hydrophobic sub-pocket and forms the hydrophobic interaction with Ile86 and the electrostatic interaction with Asp81. This plausible binding mode generally complies with

the bioassay data, which showed that the substitutions of the thiazol-2-yl group caused minor variations in GyrB inhibition instead of significant changes.

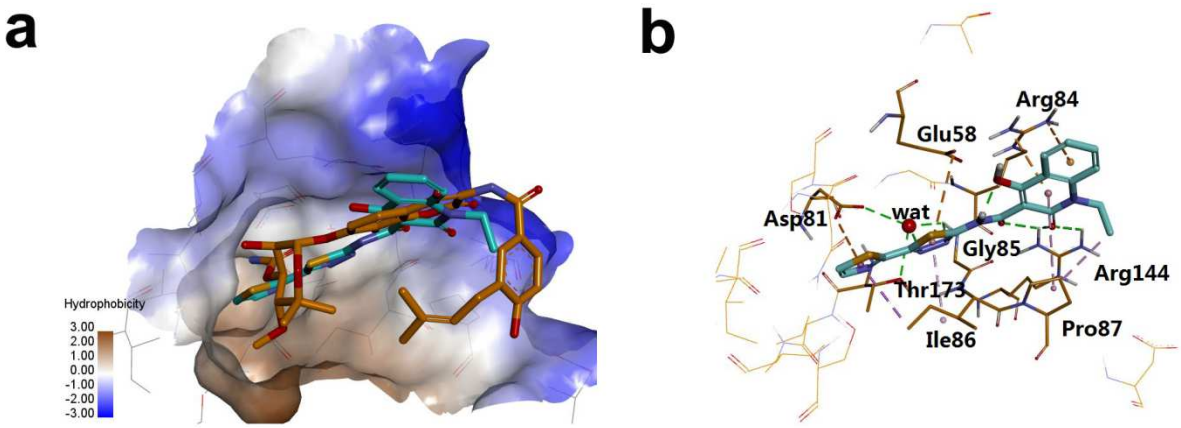

Figure 6. Potential binding modes of **g37** to the ATP binding site of *S. aureus* GyrB (PDB code: 4URO) as derived by molecular docking with OEDocking. Images were created with Discovery Studio 2017. (a) Surface representation of the ATP binding site where **g37** is located. Color codes: blue, g37; orange, novobiocin. (b) Detailed view of interactions between **g37** and GyrB. The interacting atoms and **g37** are shown in stick representations.

3. Conclusion

Antibiotic resistance has become a threat to public health worldwide [34]. It is well known that one of the potential solutions to the antibiotic resistance crisis is the use of alternative drugs structurally different from those in clinic to treat bacterial infections. Compound **11,** identified by Peternel L. *et al.* during a high-throughput screening campaign, seems to represent a new class of antibacterial agents. However, no follow-up work has been reported on this compound so far.

Starting from compound **11**, in this work, we preliminarily explored the SAR of the N-thiadiazole-4-hydroxy-2-quinolone-3-carboxamides by the design, synthesis of 37 new

derivatives and *in vitro* evaluation of their antibacterial activities against *S. aureus* ATCC 29213. Through the efforts, we identified ten derivatives with better antibacterial activity than the reported compound **11**. Next, we focused on the determination of the most promising compound from the ten derivatives by considering both antibacterial activity spectrum and mammalian cell toxicity. Firstly, we tested them against a panel of Gram-positive bacteria including drug-resistant clinical isolates (e.g. MRSA). Most derivatives showed good antibacterial activity, of which the potencies of **g8**, **g31** and **g37** were not lower than that of the marketed antibacterial drug vancomycin for any of the tested bacterial strains. Following that, we tested the three compounds for their cytotoxicity to HepG2 and HUVEC cells and demonstrated that **g37** had the best safety among all the tested compounds.

As a drug discovery project, we comprehensively evaluated **g37** by performing a resistance development assay, time-kill kinetics analysis, *in vitro* metabolic stability test, *in vivo* pharmacokinetic profile and an *in vivo* antibacterial efficacy assay. We demonstrate that **g37** (i) did not induce the resistance development of MRSA 15-1 over 20 passages, (ii) was bactericidal rather than bacteriostatic, (iii) was metabolically stable in either mouse plasma or mouse liver microsomes, (iv) showed generally good pharmacokinetic properties in mice, (v) was orally effective in treating the mice infected with MRSA when it was prophylactically administered and was not toxic at a dose as high as 30 mg/kg. These data indicate that **g37** is worthy of further development.

Based on visual inspection of chemical structures and cheminformatics analysis, we proposed that bacterial GyrB was likely to be a target of **g37**. We then confirmed

experimentally that **g37** inhibited the ATPase activity of *S. aureus* GyrB and thus, DNA supercoiling. By testing all the other derivatives against *S. aureus* GyrB, we preliminarily uncovered the potential relationship between enzyme inhibition and antibacterial activity. By molecular docking, we derived a plausible binding mode of **g37** to *S. aureus* Gyrase B. To the best of our knowledge, this is the first report of a potential target for N-thiadiazole-4-hydroxy-2-quinolone-3-carboxamides. This interesting discovery may help the structure-guided optimization of **g37**.

In summary, this paper describes the comprehensive use of chemical synthesis, *in vitro* and *in vivo* bioassays as well as cheminformatics analysis to discover a promising antibacterial agent and its potential target. **g37** is the most potent compound of this chemical series that we have tested and its target has never been reported so far. Nevertheless, the high PPB of the compound somewhat limits its broad application. Therefore, we will continue to optimize the pharmacokinetic properties of this compound while aiming to maintain its favorable potency and safety profile.

4. Experimental

4.1. Chemistry

4.1.1. General Methods

The process of the chemical reaction was monitored by analytical thin-layer chromatography on the silica gel plates GF254 (Yantai Chemical Industry Research Institute, China). Both ^{1}H NMR (500 MHz) and ^{13}C NMR (100 MHz or 125 MHz) spectra were measured on the Bruker spectrometer (Varian Mercury, USA). The chemical shifts were recorded as the δ value (ppm), using tetramethylsilane as the internal standard. HRMS

was performed by using the Thermo Scientific™ Exactive™ Plus Mass Spectrometer (Thermo, USA). The products were purified by column chromatography on silica gel (200-300 mm; Qingdao Haiyang Chemical Co., Ltd, China). All the reagents were commercially available and used without further purification unless particularly stated.

*4.1.2. General procedure A for the synthesis of compounds **b1-b3***

The synthesis of the compounds **b1-b3** was accomplished by the following two steps. The first step was based on the method proposed by Ukrainets I. V., *et al.* [35]. At the beginning, the isatoic anhydride (1 equiv) was dissolved in dry DMF (15 mL) and the sodium hydride (1.3 equiv) was gradually added to the solution at the temperature of 0 °C. After 25 min, the halogenated compound (1.2 equiv) was also added. The reaction mixture was stirred at 45 °C and the stirring lasted for 10 h. Then, dichloromethane (15 mL) and water (15 mL) were added. The organic phase was washed with brine (15 mL), dried with magnesium sulfate and filtered. After the solvent was evaporated, the solid was recrystallized in dichloromethane/hexane to afford the desired isatoic anhydride derivative. The second step of the synthesis was based on the publication from Coppola G.M. *et al.*[36]. Diethylmalonate was added dropwise to the sodium hydride dissolved in dry DMF (15 mL) under argon atmosphere and stirred for 15 min at room temperature. Then, the mixture was added to a round-bottomed flask that contained the isatoic anhydride derivative dissolved in DMF (15 mL) under argon atmosphere. The reaction mixture was heated to 60°C and maintained at 60°C for 8 h. Following that, dichlorometane (30 mL), water (50 mL), and HCl (1 N) were added in order to adjust the pH of the mixture to 5. The organic layer was separated from the aqueous phase and washed with brine (30 mL). It

was then dried with dry magnesium sulfate and filtered. Lastly, the solvent was evaporated and the resulting solid was recrystallized in dichloromethane/hexane, which produced the compound (**b1**-**b3)**.

*4.1.2.1. Ethyl 4-hydroxy-1-methyl-2-oxo-1,2-dihydroquinoline-3-carboxylate **(b1)***

Yield 51.3%, pale yellow solid. ESI-MS (m/z): 248.13 $[M+H]^+$. ^{1}H NMR (500 MHz, DMSO-d_6) δ 8.07 (d, *J* = 7.8 Hz, 1H), 7.77 (t, *J* = 7.9 Hz, 1H), 7.54 (d, *J* = 8.6 Hz, 1H), 7.33 (t, *J* = 7.7 Hz, 1H), 4.36 (q, *J* = 7.2 Hz, 2H), 3.57 (s, 3H), 1.33 (t, *J* = 7.1 Hz, 3H).

*4.1.2.2. Ethyl 1-ethyl-4-hydroxy-2-oxo-1,2-dihydroquinoline-3-carboxylate **(b2)***

Yield 44.3%, white solid. ESI-MS (m/z): 262.21 $[M+H]^+$. ^{1}H NMR (500 MHz, DMSO-d_6) δ 13.08 (brs, 1H), 8.09 (d, *J* = 7.9 Hz, 1H), 7.76 (t, *J* = 8.0 Hz, 1H), 7.58 (d, *J* = 8.5 Hz, 1H), 7.32 (t, *J* = 7.6 Hz, 1H), 4.35 (q, *J* = 7.2 Hz, 2H), 4.24 (q, *J* = 7.2 Hz, 2H), 1.34 (t, *J* = 7.2 Hz, 3H), 1.21 (t, *J* = 7.1 Hz, 3H).

*4.1.2.3. Ethyl 4-hydroxy-2-oxo-1-propyl-1,2-dihydroquinoline-3-carboxylate **(b3)***

Yield 39.7%, pale yellow solid. ESI-MS (m/z): 276.34 $[M+H]^+$. ^{1}H NMR (500 MHz, DMSO-d_6) δ 13.07 (s, 1H), 8.09 (d, *J* = 8.0 Hz, 1H), 7.76 (t, *J* = 7.9 Hz, 1H), 7.58 (d, *J* = 8.7 Hz, 1H), 7.32 (t, *J* = 7.6 Hz, 1H), 4.36 (q, *J* = 7.1 Hz, 2H), 4.14 (t, *J* = 7.8 Hz, 2H), 1.62 (h, *J* = 7.6 Hz, 2H), 1.34 (t, *J* = 7.1 Hz, 3H), 0.97 (t, *J* = 7.4 Hz, 3H).

*4.1.3. General procedure B for the synthesis of compounds **c1-c3***

At first, the concentrated HCl (1.38 mL, 37%) was slowly added to the acetic anhydride (4.50 mL) at 0 °C, which yielded a solution of approximately 2.8 M HCl in acetic acid. Subsequently, the prepared solution (3 mL) of 2.8 M HCl in acetic acid was added to the ester (**b1**-**b3**, 1.00 mmol). The reaction mixture was heated to 60 °C and

refluxed at that temperature for 10 h. After the reaction mixture was cooled down to the room temperature, it was mixed with 2-propanol. The end product was obtained by filtering, washed with 2-propanol and dried in a vacuum.

4.1.3.1. 4-hydroxy-1-methyl-2-oxo-1,2-dihydroquinoline-3-carboxylic acid ***(c1)***

Yield 56.2%, white solid. ESI-MS (m/z): 218.41 $[M+H]^+$. ^{1}H NMR (500 MHz, DMSO-d_6) δ 14.42 (s, 1H), 11.34 (s, 1H), 8.19 (d, *J* = 7.9 Hz, 1H), 7.99-7.95 (m, 1H), 7.82 (d, *J* = 8.7 Hz, 1H), 7.55 (t, *J* = 7.6 Hz, 1H), 3.74 (s, 3H).

4.1.3.2 1-ethyl-4-hydroxy-2-oxo-1,2-dihydroquinoline-3-carboxylic acid ***(c2)***

Yield 61.5%, white solid. ESI-MS (m/z): 232.34 $[M-H]^+$. ^{1}H NMR (500 MHz, DMSO-d_6) δ 14.40 (brs, 1H), 8.20 (d, *J* = 8.0 Hz, 1H), 7.97 (t, *J* = 7.9 Hz, 1H), 7.89 (d, *J* = 8.7 Hz, 1H), 7.54 (t, *J* = 7.6 Hz, 1H), 4.41 (q, *J* = 7.1 Hz, 2H), 1.30 (t, *J* = 7.1 Hz, 3H).

4.1.3.3. 4-hydroxy-2-oxo-1-propyl-1,2-dihydroquinoline-3-carboxylic acid ***(c3)***

Yield 50.3%, white solid. ESI-MS (m/z): 246.12 $[M-H]^+$. ^{1}H NMR (500 MHz, DMSO-d_6) δ 14.43 (s, 1H), 11.33 (s, 1H), 8.20 (d, *J* = 7.9 Hz,1H), 7.96 (t, *J* = 7.9 Hz, 1H), 7.88 (d, *J* = 8.7 Hz, 1H), 7.54 (t, *J* = 7.6 Hz, 1H), 4.32 (t, *J* = 7.7 Hz, 2H), 1.72 (h, *J* = 7.4 Hz, 2H), 1.00 (t, *J* = 7.4 Hz, 3H).

4.1.4. General procedure C for the synthesis of compounds ***f1-35***

Trifluoroacetic acid (4 mL) was added to a mixture of nitrile (1.0 mmol) and thiosemicarbazide (1.1 mmol). The reaction mixture was stirred and refluxed for 6 h. Then, it was cooled to room temperature and aqueous ammonia was added. The precipitated solid was filtered, washed with hot water and air-dried. It should be noted that the compounds **f1-f35** were directly used for the next reaction without further purification.

4.1.4.1. 5-methyl-1,3,4-thiadiazol-2-amine ***(f1)***

Yield 82.6%, white solid. ESI-MS (m/z): 116.35 $[M+H]^+$. ^{1}H NMR (500 MHz, DMSO-d_6) δ 6.98 (s, 2H), 2.46 (s, 3H).

4.1.4.2. 5-ethyl-1,3,4-thiadiazol-2-amine ***(f2)***

Yield 55.0%, white solid. ESI-MS (m/z): 130.18 $[M+H]^+$. ^{1}H NMR (500 MHz, DMSO-d_6) δ 7.00 (s, 2H), 2.82 (q, *J* = 7.6 Hz, 2H), 1.23 (t, *J* = 7.6 Hz, 3H).

4.1.4.3. 5-propyl-1,3,4-thiadiazol-2-amine ***(f3)***

Yield 71.5%, white solid. ESI-MS (m/z): 144.26 $[M+H]^+$.^{1}H NMR (500 MHz, DMSO-d_6) δ 7.00 (s, 2H), 2.78 (t, *J* = 7.4 Hz, 2H), 1.65 (h, *J* = 7.4 Hz, 2H), 0.94 (t, *J* = 7.4 Hz, 3H).

4.1.4.4. 5-butyl-1,3,4-thiadiazol-2-amine ***(f4)***

Yield 56.3%, white solid. ESI-MS (m/z): 158.14 $[M+H]^+$. ^{1}H NMR (500 MHz, DMSO-d_6) δ 7.00 (s, 2H), 2.80 (t, *J* = 7.5 Hz, 2H), 1.61 (p, *J* = 7.5 Hz, 2H), 1.36 (h, *J* = 7.4 Hz, 2H), 0.92 (t, *J* = 7.4 Hz, 3H).

4.1.4.5. 5-pentyl-1,3,4-thiadiazol-2-amine ***(f5)***

Yield 52.9 %, white solid. ESI-MS (m/z): 172.36 $[M+H]^+$. ^{1}H NMR (500 MHz, DMSO-d_6) δ 6.99 (s, 2H), 2.80 (t, *J* = 7.5 Hz, 2H), 1.63 (t, *J* = 7.2 Hz, 2H), 1.37-1.28 (m, 4H), 0.90 (t, *J* = 6.3 Hz, 3H).

4.1.4.6. 5-hexyl-1,3,4-thiadiazol-2-amine ***(f6)***

Yield 62.1%, white solid. ESI-MS (m/z): 186.31 $[M+H]^+$. ^{1}H NMR (500 MHz, DMSO-d_6) δ 7.00 (s, 2H), 2.80 (t, *J* = 7.5 Hz, 2H), 1.62 (p, *J* = 7.4 Hz, 2H), 1.32-1.27 (m, 6H), 0.92-0.85 (m, 3H).

4.1.4.7. 5-cyclopropyl-1,3,4-thiadiazol-2-amine ***(f7)***

Yield 62.1%, white solid. ESI-MS (m/z): 142.36 $[M+H]^+$. ^1H NMR (500 MHz, DMSO-d_6) δ 7.00 (s, 2H), 2.21-2.16 (m, 1H), 1.04-1.01 (m, 2H), 0.81-0.86 (m, 2H).

4.1.4.8. 5-cyclopentyl-1,3,4-thiadiazol-2-amine ***(f8)***

Yield 61.8%, white solid. ESI-MS (m/z): 170.09 $[M+H]^+$. ^1H NMR (500 MHz, DMSO-d_6) δ 7.01 (s, 2H), 3.28 (p, *J* = 7.7 Hz, 3H), 2.04 (q, *J* = 8.4, 6.4 Hz, 5H), 1.73-1.60 (m, 1H).

4.1.4.9. 5-cyclohexyl-1,3,4-thiadiazol-2-amine ***(f9)***

Yield 55.8%, white solid. ESI-MS (m/z): 184.39 $[M+H]^+$. ^1H NMR (500 MHz, DMSO-d_6) δ 7.32 (s, 2H), 2.86 (td, *J* = 10.7, 4.3 Hz, 1H), 1.97 (d, *J* = 11.8 Hz, 2H), 1.76 (d, *J* = 12.0 Hz, 2H), 1.67 (d, *J* = 13.1 Hz, 1H), 1.48-1.31 (m, 4H), 1.24 (q, *J* = 11.9, 11.5 Hz, 1H).

4.1.4.10. 5-phenyl-1,3,4-thiadiazol-2-amine ***(f10)***

Yield 57.6%, white solid. ESI-MS (m/z): 178.21 $[M+H]^+$. ^1H NMR (500 MHz, DMSO-d_6) δ 7.79 (s, 1H), 7.77 (s, 1H), 7.53-7.46 (m, 3H), 7.43 (s, 2H).

4.1.4.11. 5-(4-fluorophenyl)-1,3,4-thiadiazol-2-amine ***(f11)***

Yield 61.2%, white solid. ESI-MS (m/z): 196.28 $[M+H]^+$. ^1H NMR (500 MHz, DMSO-d_6) δ 7.83 (dd, *J* = 8.5, 5.4 Hz, 2H), 7.44 (s, 2H), 7.34 (t, *J* = 8.7 Hz, 2H).

4.1.4.12. 5-(4-chlorophenyl)-1,3,4-thiadiazol-2-amine ***(f12)***

Yield 61.2%, white solid. ESI-MS (m/z): 212.37 $[M+H]^+$. ^1H NMR (500 MHz, DMSO-d_6) δ 7.83 (d, *J* = 8.1 Hz, 2H), 7.58 (d, *J* = 8.3 Hz, 2H), 7.53 (s, 2H).

4.1.4.13. 5-(4-bromophenyl)-1,3,4-thiadiazol-2-amine ***(f13)***

Yield 66.3%, white solid. ESI-MS (m/z): 256.47 $[M+H]^+$. ^1H NMR (500 MHz, DMSO-d_6) δ 7.73 (d, *J* = 8.3 Hz, 2H), 7.69 (d, *J* = 8.4 Hz, 2H), 7.48 (s, 2H).

4.1.4.14. 5-(4-(difluoromethoxy)phenyl)-1,3,4-thiadiazol-2-amine ***(f14)***

Yield 48.8 %, white solid. ESI-MS (m/z): 244.41 $[M+H]^+$. ^1H NMR (500 MHz, DMSO-d_6) δ 7.84 (d, *J* = 8.3 Hz,2H), 7.44 (s, 2H), 7.34 (s, 1H), 7.29 (d, *J* = 8.3 Hz,2H).

4.1.4.15. 5-(4-nitrophenyl)-1,3,4-thiadiazol-2-amine ***(f15)***

Yield 48.2%, white solid. ESI-MS (m/z): 223.38 $[M+H]^+$. ^1H NMR (500 MHz, DMSO-d_6) δ 8.32 (d, *J* = 8.4 Hz, 2H), 8.04 (d, *J* = 8.4 Hz, 2H), 7.75 (s, 2H).

4.1.4.16. 5-(p-tolyl)-1,3,4-thiadiazol-2-amine ***(f16)***

Yield 61.3 %, white solid. ESI-MS (m/z): 192.36 $[M+H]^+$. ^1H NMR (500 MHz, DMSO-d_6) δ 7.66 (d, *J* = 7.8 Hz, 2H), 7.38 (s, 3H), 7.30 (d, *J* = 7.9 Hz, 2H), 2.37 (s, 3H).

4.1.4.17. 5-(4-methoxyphenyl)-1,3,4-thiadiazol-2-amine ***(f17)***

Yield 87.4%, white solid. ESI-MS (m/z): 208.19 $[M+H]^+$. ^1H NMR (500 MHz, DMSO-d_6) δ 7.71 (d, *J* = 8.5 Hz, 2H), 7.31 (s, 2H), 7.05 (d, *J* = 8.4 Hz, 2H), 3.83 (s, 3H).

4.1.4.18. 5-(4-ethoxyphenyl)-1,3,4-thiadiazol-2-amine ***(f18)***

Yield 80.1%, white solid. ESI-MS (m/z): 222.42 $[M+H]^+$. ^1H NMR (500 MHz, DMSO-d_6) δ 7.70 (d, *J* = 8.4 Hz, 2H), 7.31 (s, 2H), 7.03 (d, *J* = 8.4 Hz, 2H), 4.10 (t, *J* = 7.0 Hz, 2H), 1.37 (t, *J* = 7.0 Hz, 3H).

4.1.4.19. 5-(4-(dimethylamino)phenyl)-1,3,4-thiadiazol-2-amine ***(f19)***

Yield 45.9%, white solid. ESI-MS (m/z): 221.46 $[M+H]^+$. ^1H NMR (500 MHz, DMSO-d_6) δ 7.57 (d, *J* = 8.7 Hz, 2H), 7.17 (s, 2H), 6.78 (d, *J* = 8.6 Hz, 2H), 2.99 (s, 6H).

4.1.4.20. 5-(3-fluorophenyl)-1,3,4-thiadiazol-2-amine ***(f20)***

Yield 52.8%, white solid. ESI-MS (m/z): 196.31 $[M+H]^+$. ^1H NMR (500 MHz, DMSO-d_6) δ 7.66-7.58 (m, 2H), 7.54 (s, 2H), 7.51 (d, *J* = 7.9 Hz, 1H), 7.29 (t, *J* = 8.7 Hz, 1H).

4.1.4.21. 5-(m-tolyl)-1,3,4-thiadiazol-2-amine ***(f21)***

Yield 56.0%, white solid. ESI-MS (m/z): 192.06 $[M+H]^+$. ^1H NMR (500 MHz, DMSO-d_6) δ 7.62-7.55 (m, 2H), 7.47 (s, 2H), 7.38 (t, *J* = 7.7 Hz, 1H), 7.28 (d, *J* = 7.6 Hz, 1H), 2.39 (s, 3H).

4.1.4.22. 5-(3-methoxyphenyl)-1,3,4-thiadiazol-2-amine ***(f22)***

Yield 62.3%, white solid. ESI-MS (m/z): 208.26 $[M+H]^+$. ^1H NMR (500 MHz, DMSO-d_6) δ 7.46 (s, 2H), 7.40 (t, *J* = 7.9 Hz, 1H), 7.36-7.28 (m, 2H), 7.04 (dd, *J* = 8.2, 2.5 Hz, 1H), 3.84 (s, 3H).

4.1.4.23. 5-(3-ethoxyphenyl)-1,3,4-thiadiazol-2-amine ***(f23)***

Yield 57.0%, white solid. ESI-MS (m/z): 222.61 $[M+H]^+$. ^1H NMR (500 MHz, DMSO-d_6) δ 7.44 (s, 2H), 7.39 (t, *J* = 8.0 Hz, 1H), 7.30 (d, *J* = 6.3 Hz, 2H), 7.02 (d, *J* = 8.1 Hz, 1H), 3.36 (s, 2H), 1.38 (t, *J* = 7.0 Hz, 3H).

4.1.4.24. 5-(2-fluorophenyl)-1,3,4-thiadiazol-2-amine ***(f24)***

Yield 55.9%, white solid. ESI-MS (m/z): 196.08 $[M+H]^+$. ^1H NMR (500 MHz, DMSO-d_6) δ 8.11 (t, *J* = 7.7 Hz, 1H), 7.53 (q, *J* = 7.1 Hz, 1H), 7.49 (s, 2H), 7.44-7.33 (m, 2H).

4.1.4.25. 5-(o-tolyl)-1,3,4-thiadiazol-2-amine ***(f25)***

Yield 58.1%, white solid. ESI-MS (m/z): 192.41 $[M+H]^+$. ^1H NMR (500 MHz, DMSO-d_6) δ 7.55 (d, *J* = 7.7 Hz, 1H), 7.37 (d, *J* = 5.8 Hz, 4H), 7.31 (dt, *J* = 8.7, 4.4 Hz, 1H), 2.51 (s, 3H).

4.1.4.26. 5-(2-methoxyphenyl)-1,3,4-thiadiazol-2-amine ***(f26)***

Yield 59.4%, white solid. ESI-MS (m/z): 208.09 $[M+H]^+$. ^1H NMR (500 MHz, DMSO-d_6) δ 8.12 (d, *J* = 7.7 Hz, 1H), 7.45 (t, *J* = 7.8 Hz, 1H), 7.23 (s, 1H), 7.20 (d, *J* = 7.1 Hz, 1H), 7.09 (t, *J* = 7.6 Hz, 1H), 3.96 (s, 3H).

4.1.4.27. 5-(2-ethoxyphenyl)-1,3,4-thiadiazol-2-amine ***(f27)***

Yield 57.5%, white solid. ESI-MS (m/z): 222.41 $[M+H]^+$. ^1H NMR (500 MHz, DMSO-d_6) δ 8.13 (d, *J* = 7.7 Hz, 1H), 7.58 (s, 1H), 7.46 (t, *J* = 7.8 Hz, 1H), 7.21 (d, *J* = 8.3 Hz, 1H), 7.09 (t, *J* = 7.5 Hz, 1H), 4.24 (t, *J* = 7.0 Hz, 2H), 1.49 (t, *J* = 6.9 Hz, 3H).

4.1.4.28. 5-(pyridin-2-yl)-1,3,4-thiadiazol-2-amine ***(f28)***

Yield 67.9 %, white solid. ESI-MS (m/z): 179.21 $[M+H]^+$. ^1H NMR (500 MHz, DMSO-d_6) δ 8.61 (d, *J* = 4.8 Hz, 1H), 8.07 (d, *J* = 8.1 Hz, 1H), 7.95 (d, *J* = 7.8 Hz, 1H), 7.54 (s, 2H), 7.45 (dd, *J* = 7.4, 5.0 Hz, 1H).

4.1.4.29. 5-(pyridin-3-yl)-1,3,4-thiadiazol-2-amine ***(f29)***

Yield 76.4%, white solid. ESI-MS (m/z): 179.21 $[M+H]^+$. ^1H NMR (500 MHz, DMSO-d_6) δ 8.97 (d, *J* = 2.2 Hz, 1H), 8.64 (d, *J* = 4.5 Hz, 1H), 8.16 (d, *J* = 8.1 Hz, 1H), 7.57 (s, 2H), 7.53 (dd, *J* = 8.0, 4.9 Hz, 1H).

4.1.4.30. 5-(pyridin-4-yl)-1,3,4-thiadiazol-2-amine ***(f30)***

Yield 71.9%, white solid. ESI-MS (m/z): 179.21 $[M+H]^+$. ^1H NMR (500 MHz, DMSO-d_6) δ 8.68 (d, *J* = 4.9 Hz, 2H), 7.74 (s, 2H), 7.73 (d, *J* = 4.3 Hz, 2H).

4.1.4.31. 5-(thiophen-2-yl)-1,3,4-thiadiazol-2-amine ***(f31)***

Yield 85.3 %, white solid. ESI-MS (m/z): 184.63 $[M+H]^+$. ^1H NMR (500 MHz, DMSO-d_6) δ 7.66 (d, *J* = 5.0 Hz, 1H), 7.44 (d, *J* = 5.2 Hz, 3H), 7.15 (t, *J* = 4.4 Hz, 1H).

4.1.4.32. 5-(furan-2-yl)-1,3,4-thiadiazol-2-amine ***(f32)***

Yield 90.4 %, white solid. ESI-MS (m/z): 168.26 $[M+H]^+$. ^1H NMR (500 MHz, DMSO-d_6) δ 7.85 (s, 1H), 7.47 (s, 2H), 6.97 (d, *J* = 3.3 Hz, 1H), 6.70-6.65 (m, 1H).

4.1.4.33. 5-(1-methyl-1H-pyrazol-3-yl)-1,3,4-thiadiazol-2-amine ***(f33)***

Yield54.6%, white solid. ESI-MS (m/z): 182.37 $[M+H]^+$. ^{1}H NMR (500 MHz, DMSO-d_6) δ 7.82 (d, *J* = 2.1 Hz, 1H), 7.34 (s, 2H), 6.68 (d, *J* = 2.3 Hz, 1H), 3.90 (s, 3H).

4.1.4.34. 5-(thiazol-4-yl)-1,3,4-thiadiazol-2-amine ***(f34)***

Yield 72.3%, white solid. ESI-MS (m/z): 185.37 $[M+H]^+$. ^{1}H NMR (500 MHz, DMSO-d_6) δ 9.23 (s, 1H), 8.23 (s, 1H), 7.45 (s, 2H).

4.1.4.35. 5-(thiazol-2-yl)-1,3,4-thiadiazol-2-amine ***(f35)***

Yield 63.2%, white solid. ESI-MS (m/z): 185.37 $[M+H]^+$. ^{1}H NMR (500 MHz, DMSO-d_6) δ 7.96 (d, *J* = 3.2 Hz, 1H), 7.86 (d, *J* = 3.1 Hz, 1H), 7.74 (s, 2H).

4.1.5. General procedure D for the synthesis of compounds ***g1-g37***

EDCI (1.5 equiv) was added to a solution of the acid (**c1-c3**, 1.1 equiv), DIPEA (1.5 equiv) and HOBt (1.5 equiv) in DMF (10 mL) at 0°C and stirred for 5 min. Then, the amine (**f1-f35**, 1.0 equiv) was added to the solution and the reaction mixture was stirred for 48 h at room temperature. The mixture was poured into the iced water. The precipitated solid was filtered and washed with iced water. After the purification by a silica gel column chromatography, the target compound (**11** or **g1-g37**) was produced.

*4.1.5.1.1-methyl-N-(5-ethyl-1,3,4-thiadiazol-2-yl)-4-hydroxy-2-oxo-1,2-dihydroquinoline-3-carboxamide (**11**)*

Yield 14.1 %, light yellow solid. ESI-MS (m/z): 331.11$[M+H]^+$. ^{1}H NMR (400 MHz, DMSO-d_6) δ 8.28-8.23 (m, 0H), 7.87-7.84 (m, 1H), 7.74-7.69 (m, 1H), 7.51-7.44 (m, 1H), 7.32 (dd, *J* = 16.5, 8.5 Hz, 1H), 3.60 (s, 3H), 1.29-1.17 (m, 2H), 0.98-0.85 (m, 3H). ^{13}C NMR (100 MHz, DMSO-d_6) δ 162.77, 161.79, 161.38, 143.29, 140.25, 133.39, 130.37, 123.04, 120.84, 115.87, 109.55, 98.89, 36.24, 29.68, 14.14. HRMS calcd for $C_{15}H_{15}N_4O_3S$ $[M+H]^+$, 331.0865; found, 331.0859.

4.1.5.2.4-hydroxy-1-methyl-2-oxo-N-(1,3,4-thiadiazol-2-yl)-1,2-dihydroquinoline-3-carbox amide ***(g1)***

Yield 13.6 %, white solid. ESI-MS (m/z): 303.28 $[M+H]^+$. ^{1}H NMR (500 MHz, DMSO-d_6) δ 9.04 (d, *J* = 6.1 Hz, 1H), 8.29-8.13 (m, 1H), 7.77-7.45 (m, 1H), 7.40-7.11 (m, 2H), 3.53 (s, 3H). ^{13}C NMR (100 MHz, DMSO-d_6) δ 176.97, 167.80, 165.87, 163.73, 159.26, 140.73, 132.37, 126.55, 122.13, 120.83, 114.35, 97.32, 28.72. HRMS calcd for $C_{13}H_{11}N_4O_3S$ $[M+H]^+$, 303.3031; found, 303.3041.

*4.1.5.3.1-ethyl-4-hydroxy-2-oxo-N-(1,3,4-thiadiazol-2-yl)-1,2-dihydroquinoline-3-carboxa mide (****g2****)*

Yield 11.7%, white solid. ESI-MS (m/z): 317.29 $[M+H]^+$. ^{1}H NMR (500 MHz, DMSO-d_6) δ 9.04 (s, 1H), 8.21 (d, *J* = 7.8 Hz, 1H), 7.58 (t, *J* = 7.8 Hz, 1H), 7.38 (d, *J* = 8.4 Hz, 1H), 7.15 (t, *J* = 7.5 Hz, 1H), 4.22 (d, *J* = 7.6 Hz, 2H), 1.22-1.18 (m, 3H). ^{13}C NMR (100 MHz, DMSO-d_6) δ 176.97, 166.13, 163.56, 160.98, 159.23, 139.58, 132.50, 126.88, 122.94, 122.48, 114.20, 98.88, 35.92, 13.45. HRMS calcd for $C_{14}H_{13}N_4O_3S$ $[M+H]^+$, 317.1040; found, 317.1048.

4.1.5.4.4-hydroxy-2-oxo-1-propyl-N-(1,3,4-thiadiazol-2-yl)-1,2-dihydroquinoline-3-carbox amide ***(g3)***

Yield 17.1%, white solid. ESI-MS (m/z): 331.18 $[M+H]^+$. ^{1}H NMR (500 MHz, DMSO-d_6) δ 9.29 (s, 1H), 8.21 (d, *J* = 8.1 Hz, 1H), 7.84 (s, 1H), 7.69 (d, *J* = 21.5 Hz, 1H), 7.41 (s, 1H), 4.28 (s, 2H), 1.70 (s, 2H), 1.04-0.97 (m, 3H). ^{13}C NMR (100 MHz, DMSO-d_6) δ 177.78, 168.18, 164.97, 158.60, 149.13, 139.68, 139.26, 126.84, 126.35, 121.96, 115.37, 96.59, 37.27, 20.99, 11.48. HRMS calcd for $C_{15}H_{15}N_4O_3S$ $[M+H]^+$, 331.0852; found, 331.0864.

*4.1.5.5.1-ethyl-4-hydroxy-N-(5-methyl-1,3,4-thiadiazol-2-yl)-2-oxo-1,2-dihydroquinoline-3-carboxamide (**g4**)*

Yield 16.2%, white solid. ESI-MS (m/z): 331.13 $[M+H]^+$. ^{1}H NMR (500 MHz, DMSO-d_6) δ 7.93-7.87 (m, 1H), 7.77 (dd, *J* = 23.7, 8.2 Hz, 1H), 7.65-7.61 (m, 1H), 7.42 (d, *J* = 8.5 Hz, 1H), 4.25 (q, *J* = 7.1 Hz, 2H), 1.22 (t, *J* = 7.2 Hz, 6H). ^{13}C NMR (100 MHz, DMSO-d_6) δ 177.73, 167.63, 165.17, 164.90, 162.78, 133.68, 126.94, 123.11, 122.08, 115.30, 112.82, 95.91, 36.93, 19.31, 13.43. HRMS calcd for $C_{15}H_{15}N_4O_3S$ $[M+H]^+$, 331.1390; found, 331.1411.

*4.1.5.6.1-ethyl-N-(5-ethyl-1,3,4-thiadiazol-2-yl)-4-hydroxy-2-oxo-1,2-dihydroquinoline-3-carboxamide (**g5**)*

Yield 11.6 %, white solid. ESI-MS (m/z): 345.09 $[M+H]^+$. ^{1}H NMR (500 MHz, DMSO-d_6) δ 8.21 (d, *J* = 7.6 Hz, 1H), 7.58 (t, *J* = 7.7 Hz, 1H), 7.39 (d, *J* = 8.5 Hz, 1H), 7.15 (d, *J* = 7.6 Hz, 1H), 4.23 (q, *J* = 7.2 Hz, 2H), 2.92 (s, 2H), 1.20 (t, *J* = 7.1 Hz, 6H). ^{13}C NMR (126 MHz, DMSO-d_6) δ 174.63, 166.31, 163.91, 163.01, 159.09, 139.67, 132.80, 127.06, 126.65, 122.21, 114.49, 97.30, 36.45, 31.42, 23.27, 13.59. HRMS calcd for $C_{16}H_{17}N_4O_3S$ $[M+H]^+$, 345.2236; found, 345.2206.

*4.1.5.7.1-ethyl-4-hydroxy-2-oxo-N-(5-propyl-1,3,4-thiadiazol-2-yl)-1,2-dihydroquinoline-3-carboxamide (**g6**)*

Yield 20.9%, white solid. ESI-MS (m/z): 359.11 $[M+H]^+$. ^{1}H NMR (500 MHz, DMSO-d_6) δ 8.21 (t, *J* = 8.0 Hz, 1H), 7.64 (t, *J* = 7.4 Hz, 1H), 7.57-7.41 (m, 2H), 7.22 (d, *J* = 7.6 Hz, 1H), 4.26 (q, *J* = 7.8 Hz, 2H), 1.24-1.19 (m, 7H), 0.96 (s, 3H). ^{13}C NMR (100 MHz, DMSO-d_6) δ 177.73, 164.58, 161.83, 160.97, 158.70, 143.29, 133.49, 130.38, 122.94,

120.84, 109.62, 98.88, 37.22, 31.36, 23.05, 13.87, 13.38. HRMS calcd for $C_{17}H_{19}N_4O_3S$ $[M+H]^+$, 359.0956; found, 359.0968.

*4.1.5.8.N-(5-butyl-1,3,4-thiadiazol-2-yl)-1-ethyl-4-hydroxy-2-oxo-1,2-dihydroquinoline-3-carboxamide (**g7**)*

Yield 18.5%, white solid. ESI-MS (m/z): 373.09 $[M+H]^+$. ^{1}H NMR (500 MHz, DMSO-d_6) δ 8.24 (dd, *J* = 18.4, 10.6 Hz, 1H), 7.69 (d, *J* = 20.2 Hz, 2H), 7.53 (t, *J* = 7.9 Hz, 1H), 7.32-7.25 (m, 1H), 4.30 (q, *J* = 7.1 Hz, 2H), 1.36-1.12 (m, 9H), 0.93-0.72 (m, 3H). ^{13}C NMR (125 MHz, DMSO-d_6) δ 176.97, 165.96, 163.52, 159.18, 153.96, 139.78, 132.59, 127.04, 122.69, 120.82, 114.31, 97.38, 36.04, 32.00, 29.31, 22.22, 14.26, 13.63. HRMS calcd for $C_{18}H_{21}N_4O_3S$ $[M+H]^+$, 373.1319; found, 373.1329.

*4.1.5.9.1-ethyl-4-hydroxy-2-oxo-N-(5-pentyl-1,3,4-thiadiazol-2-yl)-1,2-dihydroquinoline-3-carboxamide (**g8**)*

Yield 21.8%, white solid. ESI-MS (m/z): 386.93.01 $[M+H]^+$. ^{1}H NMR (500 MHz, DMSO-d_6) δ 8.21 (d, *J* = 7.8 Hz, 1H), 7.58 (t, *J* = 7.8 Hz, 1H), 7.39 (d, *J* = 8.5 Hz, 1H), 7.16 (t, *J* = 7.5 Hz, 1H), 4.23 (q, *J* = 7.6 Hz, 2H), 2.92 (s, 2H), 1.69 (s, 2H), 1.21 (t, *J* = 6.8 Hz, 7H), 0.88 (s, 3H). ^{13}C NMR (125 MHz, DMSO-d_6) δ 177.13, 166.33, 163.88, 163.54, 159.13, 139.68, 132.74, 127.05, 122.66, 121.03, 114.44, 97.30, 37.09, 31.23, 29.59, 22.41, 22.18, 14.47, 13.61. HRMS calcd for $C_{19}H_{23}N_4O_3S$ $[M+H]^+$, 386.9765; found, 386.9774.

*4.1.5.10.1-ethyl-4-hydroxy-2-oxo-N-(5-hexyl-1,3,4-thiadiazol-2-yl)-1,2-dihydroquinoline-3-carboxamide (**g9**)*

Yield 16.5%, white solid. ESI-MS (m/z): 401.12 $[M+H]^+$. ^{1}H NMR (500 MHz, DMSO-d_6) δ 8.21 (d, *J* = 7.9 Hz, 1H), 7.58 (t, *J* = 7.8 Hz, 1H), 7.39 (d, *J* = 8.5 Hz, 1H), 7.16 (d, *J* =

7.6 Hz, 1H), 4.23 (q, *J* = 7.1 Hz, 2H), 1.36-1.10 (m, 13H), 0.86 (t, *J*= 7.1 Hz, 3H). ^{13}C NMR (100 MHz, DMSO-d_6) δ 176.94, 166.16, 164.68, 163.71, 158.93, 139.50, 132.54, 126.89, 122.50, 120.83, 114.25, 97.10, 36.02, 31.31, 29.66, 29.41, 28.51, 22.43, 14.36, 13.40. HRMS calcd for $C_{20}H_{25}N_4O_3S$ $[M+H]^+$, 401.1637; found, 401.1642.

*4.1.5.11.N-(5-cyclopropyl-1,3,4-thiadiazol-2-yl)-1-ethyl-4-hydroxy-2-oxo-1,2-dihydroquinoline-3-carboxamide (**g10**)*

Yield 19.1%, white solid. ESI-MS (m/z): 357.17 $[M+H]^+$. ^{1}H NMR (500 MHz, DMSO-d_6) δ 8.16-8.06 (m, 1H), 7.68 (m, 1H), 7.44 (s, 1H), 7.35-7.22 (m, 1H), 4.41-4.21 (m, 2H), 2.91 (s, 1H), 2.75 (s, 1H), 1.28-1.12 (m, 6H). ^{13}C NMR (100 MHz, DMSO-d_6) δ 166.71, 161.74, 160.92, 157.24, 148.62, 139.40, 138.99, 133.55, 126.72, 123.19, 114.85, 96.80, 37.22, 13.31, 10.91, 10.16. HRMS calcd for $C_{17}H_{16}N_4O_3S$ $[M+H]^+$, 357.2972; found, 357.2964.

*4.1.5.12.N-(5-cyclopentyl-1,3,4-thiadiazol-2-yl)-1-ethyl-4-hydroxy-2-oxo-1,2-dihydroquinoline-3-carboxamide **(g11)***

Yield 19.7%, white solid. ESI-MS (m/z): 385.31 $[M+H]^+$. ^{1}H NMR (500 MHz, DMSO-d_6) δ 8.28 (dd, *J* = 8.3, 3.1 Hz, 1H), 7.93-7.85 (m, 1H), 7.78-7.73 (m, 1H),, 7.63 (t, *J* = 7.8 Hz, 1H), 4.29 (q, *J* = 7.0 Hz, 2H), 2.04 (q, *J* = 9.0, 6.7 Hz, 3H), 1.76-1.66 (m, 6H), 1.23 (t, *J* = 7.1 Hz, 3H). ^{13}C NMR (125 MHz, DMSO-d_6) δ 170.19, 168.63, 163.69, 163.25, 163.03, 139.67, 130.00, 128.49, 126.65, 119.57, 113.49, 36.07, 33.76, 31.43, 25.43, 13.93. HRMS calcd for $C_{19}H_{21}N_4O_3S$ $[M+H]^+$, 385.1320; found, 385.1329.

*4.1.5.13.N-(5-cyclohexyl-1,3,4-thiadiazol-2-yl)-1-ethyl-4-hydroxy-2-oxo-1,2-dihydroquinoline-3-carboxamide **(g12)***

Yield 15.1%, white solid. ESI-MS (m/z): 399.32 $[M+H]^+$. ^{1}H NMR (500 MHz, DMSO-d_6) δ 7.93-7.85 (m, 1H), 7.78 (d, *J* = 8.5 Hz, 1H), 7.63 (t, *J* = 7.8 Hz, 1H), 7.50 (t, *J* = 8.3, 7.5 Hz, 1H), 4.28 (d, *J* = 7.6 Hz, 1H), 2.75 (s, 1H), 1.96 (m, 2H), 1.75 (m, 2H), 1.39 (m, 6H), 1.25-1.18 (m, 3H). ^{13}C NMR (100 MHz, DMSO-d_6) δ 168.12, 164.06, 161.83, 160.97, 143.28, 139.23, 133.48, 130.37, 122.93, 115.61, 109.60, 98.87, 37.23, 36.24, 33.44, 31.23, 25.82, 13.12. HRMS calcd for $C_{20}H_{23}N_4O_3S$ $[M+H]^+$, 399.3468; found, 399.3477.

4.1.5.14.1-ethyl-4-hydroxy-2-oxo-N-(5-phenyl-1,3,4-thiadiazol-2-yl)-1,2-dihydroquinoline-3-carboxamide ***(g13)***

Yield 15.8%, light yellow solid. ESI-MS (m/z): 393.08 $[M+H]^+$. ^{1}H NMR (500 MHz, DMSO-d_6) δ 8.24 (s, 1H), 8.02 (s, 2H), 7.91 (s, 1H), 7.78 (s, 1H), 7.59 (s, 3H), 7.47 (s, 1H), 4.42 (s, 2H), 1.31 (s, 3H). ^{13}C NMR (100 MHz, DMSO-d_6) δ 168.98, 164.73, 161.83, 160.97, 156.81, 143.28, 133.48, 129.60, 126.77, 126.36, 122.94, 120.84, 115.62, 112.47, 109.62, 98.88, 37.22, 13.12. HRMS calcd for $C_{20}H_{17}N_4O_3S$ $[M+H]^+$, 393.1002; found, 393.1016.

4.1.5.15.1-ethyl-N-(5-(4-fluorophenyl)-1,3,4-thiadiazol-2-yl)-4-hydroxy-2-oxo-1,2-dihydroquinoline-3-carboxamide ***(g14)***

Yield 13.4 %, white solid. ESI-MS (m/z): 411.14 $[M+H]^+$. ^{1}H NMR (500 MHz, DMSO-d_6) δ 7.90 (t, *J* = 9.1 Hz, 1H), 7.83 (dd, *J* = 8.5, 5.4 Hz, 2H), 7.80-7.73 (m, 1H), 7.44 (s, 2H), 7.34 (t, *J* = 8.7 Hz, 2H), 4.29 (q, *J* = 7.1 Hz, 2H), 1.23 (t, *J* = 7.2 Hz, 3H). ^{13}C NMR (125 MHz, DMSO-d_6) δ 169.28, 164.29, 163.04, 162.32, 155.93, 139.57, 130.29, 129.16, 128.19, 126.40, 123.50, 119.89, 116.92, 116.74, 113.69, 103.28, 36.24, 13.87. HRMS calcd for $C_{20}H_{16}FN_4O_3S$ $[M+H]^+$, 411.0912; found, 411.0911.

4.1.5.16.N-(5-(4-chlorophenyl)-1,3,4-thiadiazol-2-yl)-1-ethyl-4-hydroxy-2-oxo-1,2-dihydro quinoline-3-carboxamide ***(g15)***

Yield 16.4 %, white solid. ESI-MS (m/z): 427.12 $[M+H]^+$. ^{1}H NMR (500 MHz, DMSO-d_6) δ 7.80 (d, *J* = 8.2 Hz, 2H), 7.55 (d, *J* = 8.3 Hz, 3H), 7.50 (s, 3H), 4.27 (dd, *J* = 19.5, 12.3 Hz, 2H), 1.22 (t, *J* = 7.1 Hz, 3H). ^{13}C NMR (125 MHz, DMSO-d_6) δ 170.20, 169.51, 163.25, 163.03, 155.80, 139.68, 134.63, 130.45, 129.84, 128.57, 126.66, 123.27, 121.20, 119.57, 113.49, 102.47, 36.47, 13.93. HRMS calcd for $C_{20}H_{16}ClN_4O_3S$ $[M+H]^+$, 427.0618; found, 427.0618.

4.1.5.17.N-(5-(4-bromophenyl)-1,3,4-thiadiazol-2-yl)-1-ethyl-4-hydroxy-2-oxo-1,2-dihydro quinoline-3-carboxamide ***(g16)***

Yield 15.6 %, white solid. ESI-MS (m/z): 472.31 $[M+H]^+$. ^{1}H NMR (500 MHz, DMSO-d_6) δ 7.73 (d, *J* = 8.5 Hz, 2H), 7.69 (d, *J* = 8.4 Hz, 3H), 7.51 (s, 3H), 4.30 (p, *J* = 6.8 Hz, 2H), 1.23 (t, *J* = 7.1 Hz, 3H). ^{13}C NMR (125 MHz, DMSO-d_6) δ 169.51, 166.72, 163.22, 162.18, 155.88, 139.17, 132.74, 131.52, 130.79, 128.78, 125.33, 124.44, 123.30, 121.26, 114.52, 99.00, 36.95, 13.63. HRMS calcd for $C_{20}H_{16}BrN_4O_3S$ $[M+H]^+$, 472.0145; found, 472.0146.

4.1.5.18.N-(5-(4-(difluoromethoxy)phenyl)-1,3,4-thiadiazol-2-yl)-1-ethyl-4-hydroxy-2-oxo-1,2-dihydroquinoline-3-carboxamide ***(g17)***

Yield 11.2 %, white solid. ESI-MS (m/z): 459.84 $[M+H]^+$. ^{1}H NMR (500 MHz, DMSO-d_6) δ 8.24 (dd, *J* = 14.7, 7.3 Hz, 1H), 7.89-7.81 (m, 1H), 7.71 (d, *J* = 8.4 Hz, 1H), 7.60 (dd, *J* = 13.2, 7.6 Hz, 1H), 7.51-7.39 (m, 2H), 7.37-7.29 (m, 2H), 7.19 (d, *J* = 12.4 Hz, 1H), 4.26 (dd, *J* = 15.6, 7.9 Hz, 2H), 1.23-1.17 (m, 3H). ^{13}C NMR (125 MHz, DMSO-d_6) δ 166.54, 162.99, 160.57, 159.32, 152.61, 139.64, 133.14, 132.09, 128.69, 127.07, 124.81, 119.80,

118.80, 116.74, 114.69, 97.13, 37.06, 13.50. HRMS calcd for $C_{23}H_{23}N_4O_4S$ $[M+H]^+$, 460.1884; found, 460.1876.

4.1.5.19.1-ethyl-4-hydroxy-N-(5-(4-nitrophenyl)-1,3,4-thiadiazol-2-yl)-2-oxo-1,2-dihydroquinoline-3-carboxamide ***(g18)***

Yield 18.4 %, white solid. ESI-MS (m/z): 438.12 $[M+H]^+$. ^{1}H NMR (500 MHz, DMSO-d_6) δ 8.32 (d, *J* = 8.4 Hz, 3H), 8.04 (d, *J* = 8.5 Hz, 2H), 7.76 (s, 3H), 4.29 (q, *J* = 7.1 Hz, 2H), 1.22 (t, *J* = 7.0 Hz, 3H). ^{13}C NMR (125 MHz, DMSO-d_6) δ 170.68, 165.96, 163.22, 163.02, 154.76, 148.02, 139.67, 137.44, 130.04, 128.50, 127.76, 125.11, 124.63, 119.62, 113.52, 98.42, 37.09, 13.92. HRMS calcd for $C_{20}H_{16}N_5O_5S$ $[M+H]^+$, 438.1327; found, 438.1336.

4.1.5.20.1-ethyl-4-hydroxy-2-oxo-N-(5-(p-tolyl)-1,3,4-thiadiazol-2-yl)-1,2-dihydroquinoline-3-carboxamide ***(g19)***

Yield 20.1 %, white solid. ESI-MS (m/z): 407.19 $[M+H]^+$. ^{1}H NMR (500 MHz, DMSO-d_6) δ 7.90 (t, *J* = 8.8 Hz, 1H), 7.81-7.73 (m, 1H), 7.66 (d, *J* = 7.9 Hz, 2H), 7.37 (s, 2H), 7.30 (d, *J* = 7.9 Hz, 2H), 4.30 (p, *J* = 7.2, 6.4 Hz, 2H), 2.37 (s, 3H), 1.23 (t, *J* = 7.1 Hz, 3H). ^{13}C NMR (125 MHz, DMSO-d_6) δ 170.62, 168.85, 164.21, 161.99, 157.16, 148.18, 140.00, 139.08, 131.79, 130.33, 128.91, 126.90, 125.09, 121.57, 114.71, 97.34, 37.11, 21.55, 13.58. HRMS calcd for $C_{21}H_{19}N_4O_3S$ $[M+H]^+$, 407.1162; found, 407.1162.

4.1.5.21.1-ethyl-4-hydroxy-N-(5-(4-methoxyphenyl)-1,3,4-thiadiazol-2-yl)-2-oxo-1,2-dihydroquinoline-3-carboxamide ***(g20)***

Yield 22.9 %, white solid. ESI-MS (m/z): 423.43 $[M+H]^+$. ^{1}H NMR (500 MHz, DMSO-d_6) δ 8.28 (dd, *J* = 8.2, 4.1 Hz, 1H), 7.94-7.85 (m, 1H), 7.80-7.74 (m, 1H), 7.72 (s, 2H), 7.31 (s, 2H), 7.05 (d, *J* = 8.5 Hz, 2H), 4.29 (q, *J* = 7.1 Hz, 2H), 3.84 (s, 3H), 1.27-1.22 (m, 3H). ^{13}C

NMR (125 MHz, DMSO-d_6) δ 168.54, 163.03, 160.93, 156.96, 138.99, 132.06, 128.48, 124.87, 124.23, 123.70, 121.86, 120.97, 115.70, 115.16, 114.89, 98.65, 55.97, 36.46, 13.53. HRMS calcd for $C_{21}H_{19}N_4O_4S$ $[M+H]^+$, 423.1111; found, 423.1122.

4.1.5.22.N-(5-(4-ethoxyphenyl)-1,3,4-thiadiazol-2-yl)-1-ethyl-4-hydroxy-2-oxo-1,2-dihydro quinoline-3-carboxamide ***(g21)***

Yield 18.6 %, white solid. ESI-MS (m/z): 437.16 $[M+H]^+$. ^{1}H NMR (500 MHz, DMSO-d_6) δ 7.68 (d, *J* = 8.4 Hz, 2H), 7.30 (s, 4H), 7.02 (d, *J* = 8.4 Hz, 2H), 4.28 (q, *J* = 7.1 Hz, 2H), 4.09 (q, *J* = 6.9 Hz, 2H), 1.36 (t, *J* = 7.0 Hz, 3H), 1.22 (t, *J* = 7.1 Hz, 3H). ^{13}C NMR (125 MHz, DMSO-d_6) δ 168.32, 162.82, 160.02, 156.78, 139.07, 134.67, 128.28, 125.36, 124.04, 123.90, 120.80, 115.37, 98.08, 63.75, 36.62, 15.03, 13.50. HRMS calcd for $C_{22}H_{21}N_4O_4S$ $[M+H]^+$, 437.1269; found, 437.1278.

4.1.5.23.N-(5-(4-(dimethylamino)phenyl)-1,3,4-thiadiazol-2-yl)-1-ethyl-4-hydroxy-2-oxo-1, 2-dihydroquinoline-3-carboxamide ***(g22)***

Yield 8.2%, white solid. ESI-MS (m/z): 436.09 $[M+H]^+$. ^{1}H NMR (500 MHz, DMSO-d_6) δ 7.57 (d, *J* = 8.5 Hz, 2H), 7.18 (s, 3H), 6.77 (d, *J* = 8.5 Hz, 3H), 4.27 (tt, *J* = 23.3, 17.0, 12.1 Hz, 2H), 2.98 (s, 6H), 1.21 (dt, *J* = 14.3, 7.2 Hz, 3H). ^{13}C NMR (125 MHz, DMSO-d_6) δ 167.62, 164.31, 163.02, 157.96, 151.66, 139.58, 133.81, 130.29, 128.06, 126.41, 125.06, 123.49, 119.13, 113.68, 112.59, 96.30, 36.45, 31.42, 13.87. HRMS calcd for $C_{22}H_{22}N_5O_3S$ $[M+H]^+$, 436.1428; found, 436.1438.

4.1.5.24.1-ethyl-N-(5-(3-fluorophenyl)-1,3,4-thiadiazol-2-yl)-4-hydroxy-2-oxo-1,2-dihydroq uinoline-3-carboxamide ***(g23)***

Yield 15.8%, white solid. ESI-MS (m/z): 411.06 $[M+H]^+$. ^{1}H NMR (500 MHz, DMSO-d_6) δ 7.92-7.87 (m, 1H), 7.80-7.73 (m, 1H), 7.62 (d, *J* = 8.4 Hz, 2H), 7.54 (s, 2H), 7.31 (t, *J* = 8.8 Hz, 2H), 4.29 (q, *J* = 7.0 Hz, 2H), 1.23 (t, *J* = 7.1 Hz, 3H). ^{13}C NMR (125 MHz, DMSO-d_6) δ 169.52, 163.77, 163.06, 161.83, 155.49, 139.49, 133.59, 131.84, 129.81, 128.32, 126.46, 124.29, 123.12, 119.39, 116.89, 113.30, 113.07, 102.28, 35.88, 13.74. HRMS calcd for $C_{20}H_{16}FN_4O_3S$ $[M+H]^+$, 411.0912; found, 411.0911.

4.1.5.25.1-ethyl-4-hydroxy-2-oxo-N-(5-(m-tolyl)-1,3,4-thiadiazol-2-yl)-1,2-dihydroquinoline-3-carboxamide ***(g24)***

Yield 10.8%, white solid. ESI-MS (m/z): 407.09 $[M+H]^+$. ^{1}H NMR (500 MHz, DMSO-d_6) δ 7.60 (s, 1H), 7.57 (d, *J* = 7.8 Hz, 1H), 7.37 (t, *J* = 7.7 Hz, 1H), 7.27 (d, *J* = 7.7 Hz, 1H), 4.29 (q, *J* = 7.2 Hz, 2H), 2.38 (s, 3H), 1.24-1.20 (m, 3H). ^{13}C NMR (125 MHz, DMSO-d_6) δ 169.08, 165.67, 161.73, 157.16, 153.29, 139.14, 138.96, 132.14, 131.54, 130.92, 129.68, 127.39, 124.78, 124.17, 121.95, 114.93, 99.22, 37.32, 21.52, 13.51. HRMS calcd for $C_{21}H_{19}N_4O_3S$ $[M+H]^+$, 407.1161; found, 407.1172.

4.1.5.26.1-ethyl-4-hydroxy-N-(5-(3-methoxyphenyl)-1,3,4-thiadiazol-2-yl)-2-oxo-1,2-dihydroquinoline-3-carboxamide ***(g25)***

Yield 16.3%, white solid. ESI-MS (m/z): 423.21 $[M+H]^+$. ^{1}H NMR (500 MHz, DMSO-d_6) δ 8.28 (dd, *J* = 8.3, 3.9 Hz, 1H), 7.94-7.86 (m, 1H), 7.81-7.72 (m, 1H), 7.41 (t, *J* = 7.9 Hz, 2H), 7.35-7.29 (m, 3H), 7.04 (dd, *J* = 8.2, 2.5 Hz, 2H), 4.29 (q, *J* = 7.1 Hz, 2H), 3.85 (s, 3H), 1.23 (t, *J* = 7.1 Hz, 3H). ^{13}C NMR (125 MHz, DMSO-d_6) δ 169.07, 161.60, 160.02, 156.65, 138.80, 132.66, 131.90, 130.83, 124.65, 123.15, 121.70, 119.51, 117.18, 116.02,

114.71, 111.23, 108.04, 98.81, 55.71, 37.10, 13.34. HRMS calcd for $C_{21}H_{19}N_4O_4S$ $[M+H]^+$, 423.1111; found, 423.1122.

4.1.5.27.N-(5-(3-ethoxyphenyl)-1,3,4-thiadiazol-2-yl)-1-ethyl-4-hydroxy-2-oxo-1,2-dihydro quinoline-3-carboxamide ***(g26)***

Yield 15.7%, white solid. ESI-MS (m/z): 437.25 $[M+H]^+$. ^{1}H NMR (500 MHz, DMSO-d_6) δ 7.45 (s, 2H), 7.39 (t, *J* = 7.9 Hz, 2H), 7.30 (d, *J* = 7.1 Hz, 2H), 7.04-6.99 (m, 2H), 4.29 (q, *J* = 7.1 Hz, 2H), 4.11 (q, *J* = 7.0 Hz, 2H), 1.37 (t, *J* = 7.0 Hz, 3H), 1.27-1.14 (m, 3H). ^{13}C NMR (125 MHz, DMSO-d_6) δ 169.05, 162.83, 162.14, 159.29, 156.69, 139.05, 132.65, 130.81, 126.90, 125.33, 124.08, 120.84, 119.34, 116.96, 116.38, 114.18, 111.79, 96.95, 63.68, 36.27, 15.06, 13.49. HRMS calcd for $C_{22}H_{21}N_4O_4S$ $[M+H]^+$, 437.1269; found, 437.1278.

4.1.5.28.1-ethyl-N-(5-(2-fluorophenyl)-1,3,4-thiadiazol-2-yl)-4-hydroxy-2-oxo-1,2-dihydroq uinoline-3-carboxamide ***(g27)***

Yield 18.3%, white solid. ESI-MS (m/z): 411.31 $[M+H]^+$. ^{1}H NMR (500 MHz, DMSO-d_6) δ 8.28 (dd, *J* = 8.4, 4.3 Hz, 1H), 8.11 (t, *J* = 7.7 Hz, 1H), 7.92-7.85 (m, 1H), 7.80-7.72 (m, 1H), 7.51 (d, *J* = 16.4 Hz, 4H), 7.43-7.34 (m, 3H), 4.29 (q, *J* = 7.1 Hz, 2H), 1.22 (t, *J* = 7.1 Hz, 3H). ^{13}C NMR (125 MHz, DMSO-d_6) δ 177.03, 170.44, 163.06, 159.31, 157.34, 148.96, 139.50, 131.91, 129.81, 128.30, 128.14, 126.47, 125.67, 119.39, 119.17, 116.89, 113.30, 102.29, 36.91, 13.75. HRMS calcd for $C_{20}H_{16}FN_4O_3S$ $[M+H]^+$, 411.0911; found, 411.0911.

4.1.5.29.1-ethyl-4-hydroxy-2-oxo-N-(5-(o-tolyl)-1,3,4-thiadiazol-2-yl)-1,2-dihydroquinoline -3-carboxamide ***(g28)***

Yield 16.9%, white solid. ESI-MS (m/z): 407.35 $[M+H]^+$. ^{1}H NMR (500 MHz, DMSO-d_6) δ 7.92-7.85 (m, 1H), 7.76-7.70 (m, 1H), 7.55 (d, *J* = 7.5 Hz, 1H), 7.37 (d, *J* = 4.1 Hz, 3H), 7.31 (dt, *J* = 8.5, 4.3 Hz, 2H), 4.29 (q, *J* = 7.1 Hz, 2H), 2.51 (s, 3H), 1.23 (t, *J* = 7.2 Hz, 3H). ^{13}C NMR (125 MHz, DMSO-d_6) δ 169.46, 164.50, 161.72, 156.33, 153.46, 138.96, 136.51, 132.15, 132.03, 130.59, 130.40, 129.82, 126.95, 124.77, 121.97, 117.10, 114.95, 100.63, 37.32, 21.89, 13.51. HRMS calcd for $C_{21}H_{19}N_4O_3S$ $[M+H]^+$, 407.1162; found, 407.1172.

4.1.5.30.1-ethyl-4-hydroxy-N-(5-(2-methoxyphenyl)-1,3,4-thiadiazol-2-yl)-2-oxo-1,2-dihydroquinoline-3-carboxamide ***(g29)***

Yield 20.6%, white solid. ESI-MS (m/z): 423.11 $[M+H]^+$. ^{1}H NMR (500 MHz, DMSO-d_6) δ 8.28 (dd, *J* = 8.3, 3.7 Hz, 1H), 8.12 (d, *J* = 7.8 Hz, 1H), 7.93-7.86 (m, 1H), 7.81-7.72 (m, 1H), 7.50 (t, *J* = 7.5 Hz, 1H), 7.45 (t, *J* = 7.9 Hz, 1H), 7.22 (d, *J* = 8.7 Hz, 1H), 7.09 (t, *J* = 7.6 Hz, 1H), 4.29 (q, *J* = 7.0 Hz, 1H), 3.96 (s, 3H), 1.23 (t, *J* = 7.1 Hz, 3H). ^{13}C NMR (126 MHz, DMSO-d_6) δ 170.35, 162.83, 162.66, 154.97, 150.96, 139.30, 131.18, 128.51, 127.10, 126.89, 125.98, 123.51, 121.49, 120.09, 120.01, 113.68, 112.76, 98.82, 56.42, 36.28, 13.63. HRMS calcd for $C_{21}H_{19}N_4O_4S$ $[M+H]^+$, 423.1111; found, 423.1122.

4.1.5.31.N-(5-(2-ethoxyphenyl)-1,3,4-thiadiazol-2-yl)-1-ethyl-4-hydroxy-2-oxo-1,2-dihydroquinoline-3-carboxamide ***(g30)***

Yield 11.6%, white solid. ESI-MS (m/z): 437.23 $[M+H]^+$. ^{1}H NMR (500 MHz, DMSO-d_6) δ 8.15 (d, *J* = 7.7 Hz, 1H), 7.43 (t, *J* = 7.9 Hz, 1H), 7.20 (d, *J* = 4.4 Hz, 3H), 7.07 (d, *J* = 7.7 Hz, 1H), 4.32-4.27 (m, 2H), 4.24 (q, *J* = 7.0 Hz, 2H), 1.49 (t, *J* = 6.9 Hz, 3H), 1.23 (t, *J* = 7.1 Hz, 3H). ^{13}C NMR (125 MHz, DMSO-d_6) δ 170.37, 162.85, 161.87, 154.24, 151.06,

138.92, 134.73, 131.51, 131.11, 127.09, 124.98, 121.38, 121.28, 120.22, 114.45, 113.38, 95.40, 65.00, 36.87, 15.11, 13.41. HRMS calcd for $C_{22}H_{21}N_4O_4S$ $[M+H]^+$, 437.1268; found, 437.1278.

4.1.5.32.1-ethyl-4-hydroxy-2-oxo-N-(5-(pyridin-2-yl)-1,3,4-thiadiazol-2-yl)-1,2-dihydroquinoline-3-carboxamide ***(g31)***

Yield 22.8%, white solid. ESI-MS (m/z): 394.09 $[M+H]^+$. ^{1}H NMR (500 MHz, DMSO-d_6) δ 8.72-8.59 (m, 1H), 8.28 (dd, *J* = 8.3, 4.0 Hz, 1H), 8.23-8.12 (m, 1H), 8.09-7.96 (m, 1H), 7.89 (t, *J* = 9.1 Hz, 1H), 7.76 (dd, *J* = 24.3, 8.3 Hz, 1H), 7.62 (dd, *J* = 16.6, 8.4 Hz, 1H), 7.49 (q, *J* = 7.3 Hz, 1H), 4.36-4.19 (m, 2H), 1.24 (t, *J* =6.9 Hz, 3H). ^{13}C NMR (125 MHz, DMSO-d_6) δ 168.55, 162.82, 161.57, 156.27, 150.09, 148.86, 138.79, 137.48, 131.92, 124.62, 123.22, 122.39, 121.72, 117.07, 114.73, 108.13, 98.81, 37.11, 13.34. HRMS calcd for $C_{19}H_{16}N_5O_3S$ $[M+H]^+$, 394.0959; found, 394.0968.

4.1.5.33.1-ethyl-4-hydroxy-2-oxo-N-(5-(pyridin-3-yl)-1,3,4-thiadiazol-2-yl)-1,2-dihydroquinoline-3-carboxamide ***(g32)***

Yield 16.2%, white solid. ESI-MS (m/z): 394.09 $[M+H]^+$. ^{1}H NMR (500 MHz, DMSO-d_6) δ 8.28 (dd, *J* = 8.5, 4.5 Hz, 1H), 8.07 (d, *J* = 7.9 Hz, 1H), 7.93-7.85 (m, 1H), 7.76 (dd, *J* = 23.3, 8.3 Hz, 1H), 7.66-7.58 (m, 1H), 7.51 (q, *J* = 8.1, 7.6 Hz, 1H), 7.39-7.31 (m, 1H), 7.16-7.07 (m, 1H), 4.29 (q, *J* = 6.9 Hz, 2H), 1.22 (t, *J* = 7.3 Hz, 3H). ^{13}C NMR (125 MHz, DMSO-d_6) δ 170.02, 164.13, 163.06, 162.85, 158.14, 151.21, 139.49, 129.81, 128.29, 126.47, 124.85, 124.30, 119.38, 118.07, 113.58, 113.30, 98.80, 36.28, 13.75. HRMS calcd for $C_{19}H_{16}N_5O_3S$ $[M+H]^+$, 394.0959; found, 394.0968.

4.1.5.34.1-ethyl-4-hydroxy-2-oxo-N-(5-(pyridin-4-yl)-1,3,4-thiadiazol-2-yl)-1,2-dihydroquinoline-3-carboxamide ***(g33)***

Yield 17.3%, white solid. ESI-MS (m/z): 394.09 $[M+H]^+$. ^{1}H NMR (500 MHz, DMSO-d_6) δ 8.28 (dd, *J* = 8.2, 4.6 Hz, 1H), 8.08 (s, 1H), 7.93-7.86 (m, 1H), 7.81-7.72 (m, 1H), 7.64 (t, *J* = 7.8 Hz, 1H), 7.51 (t, *J* = 7.6 Hz, 1H), 7.33 (s, 1H), 7.14 (s, 1H), 4.30 (q, *J* = 7.1 Hz, 2H), 1.23 (t, *J* = 7.1 Hz, 3H). ^{13}C NMR (125 MHz, DMSO-d_6) δ 169.72, 165.56, 164.38, 163.19, 163.02, 151.16, 139.65, 130.08, 128.50, 126.60, 125.07, 123.32, 119.64, 113.53, 99.00, 36.46, 13.91. HRMS calcd for $C_{19}H_{16}N_5O_3S$ $[M+H]^+$, 394.0960; found, 394.0968.

4.1.5.35.1-ethyl-4-hydroxy-2-oxo-N-(5-(thiophen-2-yl)-1,3,4-thiadiazol-2-yl)-1,2-dihydroquinoline-3-carboxamide ***(g34)***

Yield 22.8%, grey solid. ESI-MS (m/z): 399.05 $[M+H]^+$. ^{1}H NMR (500 MHz, DMSO-d_6) δ 8.28 (dd, *J* = 8.4, 3.7 Hz, 1H), 7.90 (t, *J* = 9.3 Hz, 1H), 7.75 (dd, *J* = 15.8, 8.2 Hz, 1H), 7.68-7.61 (m, 1H), 7.50 (t, *J* = 7.7 Hz, 1H), 7.44 (d, *J* = 4.9 Hz, 1H), 4.29 (q, *J* = 7.3 Hz, 2H), 1.23 (t, *J* = 7.1 Hz, 3H). ^{13}C NMR (125 MHz, DMSO-d_6) δ 168.57, 162.82, 161.65, 158.42, 151.12, 139.42, 138.83, 133.69, 131.81, 128.46, 128.08, 126.94, 124.73, 121.60, 114.66, 96.83, 37.05, 13.36. HRMS calcd for $C_{18}H_{15}N_4O_3S_2$ $[M+H]^+$, 399.0571; found, 399.0580.

4.1.5.36.1-ethyl-4-hydroxy-N-(5-(1-methyl-1H-pyrazol-3-yl)-1,3,4-thiadiazol-2-yl)-2-oxo-1,2-dihydroquinoline-3-carboxamide ***(g35)***

Yield 18.1%, white solid. ESI-MS (m/z): 397.16 $[M+H]^+$. ^{1}H NMR (500 MHz, DMSO-d_6) δ 8.06 (d, *J* = 7.8 Hz, 2H), 7.45 (t, *J* = 7.8 Hz, 1H), 7.33 (d, *J* = 8.4 Hz, 1H), 7.11 (t, *J* = 7.5 Hz, 2H), 4.26 (s, 3H), 4.20 (q, *J* = 6.9 Hz, 2H), 1.18 (t, *J* = 7.1 Hz, 3H). ^{13}C NMR (100

MHz, DMSO-d_6) δ 169.61, 164.80, 164.04, 159.92, 158.70, 151.93, 137.88, 129.62, 124.87, 121.07, 120.25, 113.47, 112.74, 103.70, 97.13, 36.69, 25.81, 13.63. HRMS calcd for $C_{18}H_{17}N_6O_3S$ $[M+H]^+$, 397.2893; found, 397.2894.

4.1.5.37.1-ethyl-4-hydroxy-2-oxo-N-(5-(thiazol-4-yl)-1,3,4-thiadiazol-2-yl)-1,2-dihydroquinoline-3-carboxamide ***(g36)***

Yield 13.5%, white solid. ESI-MS (m/z): 400.15 $[M+H]^+$. ^{1}H NMR (500 MHz, DMSO-d_6) δ 8.15 (s, 1H), 7.48 (s, 2H), 7.38-7.10 (m, 3H), 4.30 (s, 2H), 1.32-1.16 (m, 3H). ^{13}C NMR (100 MHz, DMSO-d_6) δ 164.24, 162.78, 156.31, 155.88, 154.30, 146.77, 137.81, 131.21, 130.43, 124.91, 121.01, 117.75, 116.58, 112.67, 98.11, 36.25, 13.37. HRMS calcd for $C_{17}H_{14}N_5O_3S_2$ $[M+H]^+$, 400.0523; found,400.0533.

4.1.5.38.1-ethyl-4-hydroxy-2-oxo-N-(5-(thiazol-2-yl)-1,3,4-thiadiazol-2-yl)-1,2-dihydroquinoline-3-carboxamide ***(g37)***

Yield 18.9%, grey white solid. ESI-MS (m/z): 400.11 $[M+H]^+$. ^{1}H NMR (500 MHz, DMSO-d_6) δ 8.21 (d, J = 8.0 Hz, 1H), 8.01 (d, J = 27.5 Hz, 1H), 7.94 (d, J = 3.1 Hz, 1H), 7.58 (d, J = 8.1 Hz, 1H), 7.39 (d, J = 8.4 Hz, 1H), 7.16 (t, J = 7.5 Hz, 1H), 4.23 (q, J = 7.5 Hz, 2H), 1.22 (t, J = 7.0 Hz, 3H). ^{13}C NMR (125 MHz, DMSO-d_6) δ 177.32, 166.26, 162.99, 160.75, 159.39, 144.58, 139.83, 132.90, 127.06, 122.64, 121.07, 120.17, 114.48, 97.26, 36.45, 13.62. HRMS calcd for $C_{17}H_{14}N_5O_3S_2$ $[M+H]^+$, 400. 0523; found, 400. 0533.

4.2. Bioassays

4.2.1. Bacterial growth inhibition assay

As a primary screening, the compounds were tested against a representative bacterial strain, i.e. *S. aureus* ATCC29213. The potent compounds for *S. aureus* ATCC29213 (MIC:

less than 1 μg/mL) were submitted for a secondary screening, which covered a variety of Gram-positive clinical isolates including MRSA, MSSE, MRSE, EFA, EFM and VRE. The metrics for antibacterial activity was MIC against the corresponding bacterial strain. In this study, the broth microdilution assay recommended by the Clinical and Laboratory Standards Institute [37] was used for the screening, with levofloxacin or vancomycin as a positive control. Firstly, the compounds were dissolved in DMSO to make a stock solution at twice the maximum concentration used for the screening, i.e. 200 μg/mL for the primary screening and 128 μg/mL for the secondary screening. Then, 200 μL of the stock solution was added to the first well of the 96-well plate and 100 μL DMSO was added to the remaining 11 wells. The 2-fold serial dilution was performed to make 12 compound solutions at different concentrations. Subsequently, 100 μL of the bacterial suspension was added to each well, which produced the compound solutions at the concentrations ranging from 100 to 0.05 μg/mL or 64 to 0.03 μg/mL and the bacterial suspension at the concentration of approximately 10^5 CFU/ml. The 96-well plate was incubated at 37 °C for 18−24 h. Lastly, the concentration at which the bacterial growth was completely inhibited was determined as the MIC value of a compound by visual inspection. The assays were performed in duplicate.

4.2.2. Cytotoxicity assay

The SRB assay in cell culture was adopted to determine the effect of compounds on cell viability. The decrease of cell viability is able to reflect cytotoxicity [15]. In this study, two cell lines, i.e. HepG2 and HUVEC were used. The assay was performed in duplicate according to the protocol described below. The cells were seeded in 96-well plates and

treated with the tested compounds at nine specified concentrations ranging from10 nM to 100 μM. The cells were incubated with the tested compounds at the conditions of 37 °C and 5% CO_2 for 72 h. After that, the cells were then fixed with 10 % trichloroacetic acid (w/v) and kept at 4 °C for 1 h. The cells were then washed for five times with distilled water and then air-dried. Following that, the cells that survived were stained with 0.4% SRB and kept at room temperature for another 20 min. They were washed for five times with 1% acetic acid and then air-dried. Lastly, SRB in the bound state was solubilized with 10 mM Tris and shaked for 5 min. The optical density (OD) was recorded at the wavelength of 540 nm by using a Tecan Infinite M1000 microplate reader. The cell viability (i.e. survival rate) was calculated to measure cytotoxicity of a compound according to the following formula, i.e. survival rate (%) ={(ODcmpd-ODblank)/(ODno_cmpd-ODblank)}×100 (%). Herein, ODcmpd refers to OD of the well with the bound SRB after the compound treatment, while ODblank means OD of the well without the bound SRB. ODno_cmpd represents OD of the bound SRB without compound treatment. Based on the survival rates of the cells treated by the compounds at nine concentrations, IC_{50} values were determined using nonlinear regression with normalized dose-response fit implemented in GraphPad Prism 5 software (GraphPad Software Inc., La Jolla, CA).

4.2.3. Resistance development assay

The resistance development assay was aimed to study whether the compound may induce bacterial resistance. Prior to the assay, the compound and the positive drug, i.e. vancomycin were tested against MRSA 15-1 according to the bacterial growth inhibition

assay described above and their MIC values were determined. The suspension made up of the bacterial strain treated by the sub-MIC concentration (0.5×MIC) of the compound or vancomycin was taken and diluted to the concentration of 10^5 CFU/mL for the resistance development assay.

The resistance development assay was performed in the same way as the bacterial growth inhibition assay, except that the diluted bacterial suspension after the sub-lethal compound treatment was used. After the incubation of the bacterial strain at 37 °C for 24 h, the MIC value against the bacterial strain for this round/passage was determined. After each round, the diluted bacterial suspension after the sub-lethal compound treatment was prepared for the next-round assay. In this study, a total of 20 rounds of assays were performed and the MIC value for each round was recorded. According to the MIC viability, whether the compound induced antibiotics resistance was determined.

4.2.4 Time-kill kinetics assay

Time-kill kinetics assay was performed to determine the antimicrobial efficacy of our lead compound. The compound solutions at five concentrations, i.e. 1×MIC, 2×MIC, 4×MIC, 8×MIC and 16×MIC were respectively prepared, by adding a certain amount of the compound to 2 mL of Mueller-Hinton (MH) broth in the sterilized test tubes. Following that, 2 mL bacterial suspension (MRSA 15-1) was added to every tube. As a result, the concentrations of the compound became 0.5×MIC, 1×MIC, 2×MIC, 4×MIC and 8×MIC, while the bacterial concentration was 10^6-10^7 CFU/mL in all the tubes. As a growth control, a mixture of 2 mL MH broth and 2 mL bacterial suspension were also prepared in a sterilized test tube. All the tubes were incubated at 37 °C for 24 h.

The following measurements were performed in triplicate. At each of the following 4 time points, i.e. 0 h, 4 h, 8 h and 24 h, 1 mL of the bacterial suspension was taken and serially diluted by 10 folds with the sterilized physiological saline (0.9%NaCl). 100 μL aliquots were taken from the lower-concentration dilutions and respectively placed on the MH agar plates. The plates were incubated at 37 °C for 24 h. The number of bacterial colonies on each plate was counted. By multiplying it with ten times the dilution rate, the total number of surviving bacteria in term of $\log_{10}$ CFU/mL was calculated. To uncover the time-kill kinetics, the average of bacterial concentration ($\log_{10}$ CFU/mL) from three measurements was plotted against the incubation time.

4.2.5. Mouse plasma stability assay

The mouse plasma were purchased from BioreclamationIVT and stored at -20 °C. The test compound was dissolved in DMSO at a concentration of 10 mM, which was further diluted to a working solution (0.1 mM). The solution of the control compound, i.e. Tetracaine in DMSO (0.1 mM) was also prepared. Terfenadine (5 ng/mL) and Tolbutamide (10 ng/mL) dissolved in Methanol/CAN (1:1, v/v) were used as two internal standards (IS) solutions.

The stability of the test/control compound was measured according to the following protocol. Before use, the mouse plasma was pre-warmed at 37 °C for 15 min. Then, 4 μL of the compound/control solution was incubated with 396 μL of the mouse plasma in a 96-well plate. Subsequently, a 50 μL aliquot was taken from the reaction mixture at each of the time points, i.e. 0, 5, 15, 30, 60, 120 min (for control) or 0, 15, 30, 60, 120 min (for the test compound) and the reaction in the sample was stopped by 300 μL of IS solutions.

When the sampling was done, all the aliquots were centrifuged at 4,000 rpm at 4°C for 15min for plasma proteins sedimentation. Mixed with 100 µL of distilled water, 100 µL of the supernatant was analyzed by LC-MS/MS with Shimadzu HPLC system and the AB Sciex API 4500 QTRAP instrument. The data were analyzed by Analyst 1.6.3 software (AB Sciex). The remaining compound (%) after incubation in plasma versus the incubation time was plotted. By linear regression from the plot, the half-life ($t_{1/2}$) value of the compound was estimated.

4.2.6. Mouse microsomal stability assay

The mouse liver microsomes were purchased from BioreclamationIVT and stored at -80 °C. The working solutions of the control compound, i.e. Dextromethorphan as well as the test compound in DMSO (0.1 mM) were prepared. Similar to the plasma stability assay, Terfenadine (5ng/mL) and Tolbutamide (10 ng/mL) dissolved in Methanol/CAN (1:1, v/v) were used as two internal standards (IS) solutions. NADPH was dissolved in the phosphate buffer (50 mM K_2HPO_4, pH 7.4) at the concentration of 5 mM.

After being thawed at 37 °C, the stock solution of the mouse liver microsomes (20 mg/mL) were diluted to the concentration of 0.633 mg/mL with the phosphate buffer (50 mM K_2HPO_4, pH 7.4). 2.5 µL of the control/test compound working solution was gently mixed with 197.5 µL of the liver microsomes working solution in a 96-well plate and pre-incubated at 37°C for 5 min. To start the metabolic reaction, 50 µL of the 5mM NADPH working solution was added to the mixture. From the reaction mixture, 30 µL of aliquot was taken one by one at each of the following five time points, i.e., 0, 5, 15, 30, 60 min. The reaction in each aliquot was stopped by adding 300 µL of the IS Methanol/ACN

solution (1:1, v/v). The negative control (i.e. the assay without the metabolic reaction) was also performed, which used 50 μL of the phosphate buffer instead of the NADPH working solution. For the negative control, 30 μL of the aliquots were taken only at the time points of 0 and 60 min. Prior to LC-MS/MS analysis, each sample was mixed vigorously for about 1 min and centrifuged at 4,000 rpm at 4°C for 15 min. 100 μL of the supernatant was then taken from the sample and mixed with 100 μL of the distilled water. With the same HPLC system as the plasma stability assay, the supernatant was analyzed. The residues (%) of the test compound along with the incubation time were calculated, based on which the half-life ($t_{1/2}$) value was determined.

4.2.7. In vivo pharmacokinetics study

The Kunming mice (half male and half female) at the age of 5 to 7 weeks were used for studying pharmacokinetics properties of the test compound. The test compound was dissolved in the solvent of 0.5% CMC-Na and administered orally at a dose of 10 mg/kg. Serial specimens of the whole blood in a volume of 0.2 mL were collected from each mouse via the retro-orbital sinus at 0 min (prior to administration) and 9 time points after the administration, i.e. 0.5h, 1 h, 3 h, 6 h, 8 h, 12 h, 24 h, 48 h and 72 h. The specimens were immediately treated by K_2EDTA and then centrifuged at 8,000 rpm at 8°C for 6 min, which produced the plasma samples. The concentrations of the compound in the plasma were quantified by the same HPLC system as the *in vitro* metabolic stability assay. The curve that showed the time-dependent viability of the concentration was plotted, based on which the pharmacokinetic parameters were determined by non-compartmental analysis using Phoenix 8.1.

4.2.8. In vivo efficacy study

The Kunming mice weighing between 18 g and 22 g (half male and half female) were randomly divided into three treatment groups (n=5 per group), which were further respectively injected by three corresponding doses of the MRSA15-1 inoculum (0.5 mL), i.e. 5×10^7 CFU/mL, 5×10^6 CFU/mL and 5×10^5 CFU/mL. After the bacterial infection, the mice were observed for 7 days and the deaths were counted. The dose that led to the deaths of all the mice in that group within 7 days was considered as MLD. This dose of bacterial inoculum would be intraperitoneally injected to mice in order to establish the mouse systemic infection model.

The Kunming mice (18-22g, male: female=1:1) were randomly divided into eleven groups, with 5 or 8 mice in each group. Four treated groups (n=8 per group) were used to evaluate the orally-administered compound **g37** (9, 3, 1 and 0.33 mg/kg) for its protective effects from systemic infection. According to the dosing schedule, the mice in each group were pre-treated with the compound (solvent: 0.5% CMC-Na) at the corresponding designed dose at 12 h and 6 h before bacterial infection, respectively. The mice were then intraperitoneally injected with 0.5 mL of bacterial inoculum at the MLD. Following that, the test compound was orally administered twice at 0 h and 6 h post-infection at the same doses as the prophylactic administration. The mice were observed for 7 days and the deaths were counted, based on which the survival rate was calculated [38]. As a positive control, the *in vivo* efficacy of linezolid was also evaluated in the same way as the test compound, i.e. oral administration at the doses of 9, 3, 1 and 0.33 mg/kg. Apart from the positive drug as a control, three other controls were also set. The untreated group included the mice (n=8)

that were infected but not treated with the compound. As an alternative to the compound, they were treated with the same volume of 0.5% CMC-Na. The uninfected group represented the mice (n=5) neither infected nor treated with the compound. The mice were intraperitoneally injected with the same volume of normal saline and orally administered with the same volume of 0.5% CMC-Na. Another control represented the mice (n=5) that were not infected (with normal saline only) but treated with the test compound according to the same dosing schedule (including the prophylactic administration) as the treated group at each dose up to 30 mg/kg, which was aimed to preliminarily evaluate the toxicity of the compound. The protocol for this study was reviewed and approved by the Institutional Animal Care and Use Committee of Sichuan Primed Bio-Tech Group Co., Ltd.

4.2.9. Mouse plasma protein binding assay

The Dianorm equilibrium dialysis plate was used to determine mouse plasma protein binding. Firstly, 200 µL of the dosing solution (5 µM, the test compound dissolved in plasma) was put in the plasma chamber, while 350 µL of phosphate buffer (100 mM $NaPO_4$, 100 mM NaCl, pH 7.4) was placed in the buffer chamber. Then, the plate was sealed with an adhesive film and incubated at 37 °C for 5 h while being shaken at 100 rpm. Following that, 30 µL of aliquots were respectively taken from the plasma chamber and the buffer chamber. In order to take plasma stability into account, 30 µL of the aliquots were taken from the dosing solution (T0 sample). The aliquots (30 µL) from the plasma chamber were mixed with blank plasma (120 µL) and blank phosphate buffer (150 µL), followed by the addition of the quenching solution (600 µL), i.e. Terfenadine (5ng/mL) and Tolbutamide (10 ng/mL) dissolved in Methanol/CAN (1:1, v/v). The same protocol was

applied to the T0 sample. As for the aliquots (30 μL) from the buffer chamber, they were mixed with the blank plasma (30 μL), followed by the addition of the quenching solution (120 μL). The three mixtures were vortexed for 1 min and centrifuged at 4,000 rpm for 15 min. 100 μL of aliquots were taken from the supernatant and mixed well with distilled water (100 μL) for LC-MS/MS analysis. LC-MS/MS quantitative sample analysis was performed using an Kinetex 2.6 μm C18 100 Å column (3.0 mm×30 mm) and MRM detection (the AB Sciex API 4500 QTRAP instrument. The percentage binding was calculated based on the concentration of the compound in each sample. Warfarin was used as the positive control. The assays were performed in duplicate.

4.2.10. S. aureus GyrB inhibition assay

S. aureus Gyrase was purchased from Inspiralis Ltd (Norwich, United Kingdom). The GyrB inhibition assay required 10 μL of mixture that contained 5 nM enzyme (*S. aureus* Gyrase), buffer (40 mM HEPES-KOH (pH 7.6), 10 mM magnesium acetate, 10 mM dithiothreitol, 50 g/L BSA, 500 mM potassium glutamate), a specified concentration of the compound (0.001 μM -10 μM), 1% DMSO, 10 nM linear pBR322 DNA, 100 mM ATP. Prior to the assay, the 3-fold serial dilutions of the compound at 10 times the specified concentrations were prepared, by being dissolved in DMSO (10 mM) and diluted with the assay buffer and DMSO. For the assay, the buffer (7 μL), one of the prepared compound dilution (1 μL), the linear pBR322 DNA (0.5 μL) and *S. aureus* Gyrase (0.5 μL) was added to a PCR tube sequentially and mixed by vortex. To initiate the enzymatic reaction, ATP (1 μL) was added to the tube. The PCR tube was sealed and incubated at 37 °C for 30 min. The generated ADP was quantified by using the ADP-Glo kits. 40 μL of ADP-Glo reagent

was added to the reaction mixture and incubated at 37 °C for 40 min, which was aimed to stop the ADP-generating reaction and use up the remaining ATP. 50 μL of the detection reagent was added and mixed for 5 min. 100 μL of the mixture was transferred to 96-well plate and the luminescence (LU) was measured using a BioTek Synergy 2 microplate reader. The enzymatic activity was calculated according to the following formula, i.e. activity (%) ={(LUcmpd-LUblank)/(LUno_cmpd-LUblank)}×100 (%). Herein, LUcmpd refers to the luminescence of the mixture after the compound treatment, while LUblank means the luminescence of the mixture without ADP. ODno_cmpd represents the luminescence of the mixture without compound treatment. Based on the activity (%) of the *S. aureus* Gyrase treated by the compound at nine specified concentrations, the IC_{50} value was determined using nonlinear regression with normalized dose-response fit implemented in GraphPad Prism 5 software (GraphPad Software Inc., La Jolla, CA). Novobiocin was used as a positive control and the assays were performed in duplicate.

4.2.11. S. aureus DNA supercoiling assay

The *S. aureus* DNA supercoiling assay was mostly similar to the GyrB inhibition assay described above, except that the agarose gel electrophoresis was used to detect the status of DNA. With the same mixture (10 μL) as that for the GyrB inhibition assay in the PCR tube, the enzymatic reaction was carried out at 37 °C for 30 min. Subsequently, the sample in the PCR tube was centrifuged at 1,500 rpm for 1 min and then mixed with 2 μL of DNA loading buffer. The mixture was run through a 1% agarose gel in TAE buffer (40 mM Trisacetate, 2 mM EDTA) for 2 h at 80V. The gel was stained with ethidium bromide for 60 min, visualized and photographed under UV light.

4.2.12. S. aureus ParE inhibition assay

The *S. aureus* ParE inhibition assay was performed almost in the same way as the GyrB inhibition assay. The only difference was the 10 μL of the reaction mixture composed of 8.5 nM enzyme (*S. aureus* topoisomerase IV purchased from Inspiralis Ltd.), buffer (100 mM Tris (pH 7.5), 2 mM magnesium chloride, 1 mM dithiothreitol, 50 g/L BSA, 200 mM potassium glutamate), a specified concentration of the compound (0.01 μM-100 μM), 1% DMSO, 10 nM pBR322 DNA, 300 mM ATP. The positive control was novobiocin as well. The assay was performed in duplicate.

4.3 Molecular docking

As the compound to dock contained a core scaffold similar to the coumarin ring of novobiocin, the X-ray structure of the novobiocin-bound *S. aureus* GyrB (PDB code: 4URO) was retrieved from the Protein Data Bank (https://www.rcsb.org/). The identical protein chains, nonessential cofactors were removed from the X-ray structure. All the cocrystallized water molecules except for the conserved one potentially involved in ligand binding (i.e. wat46 [33]) were removed. Then, the protein structure was prepared by using the “Clean Protein” module in Discovery Studio 2017. The protein preparation was aimed to correct all potential problems with amino acids such as alternative conformations, nonstandard names, incomplete residues and terminus, incorrect bonds and bond orders as well as atom orders, add hydrogen atoms and generate a protonation state at pH 7.0.

A maximum of 200 conformers for the compound was generated by OMEGA (version 2.5.1.4; OpenEye Scientific Software, Inc., Santa Fe, NM, USA) [39]. The prepared protein structure was converted to a receptor ready for molecular docking by OEDocking (version

3.0.1, OpenEye Scientific Software, Inc., Santa Fe, NM, USA) [40] , in which a binding site was defined by the cognate ligand from the ligand-bound X-ray structure and an acceptor constraint on the guanidine of Arg144 was used. Then, all the conformers of the ligand structure were docked against the receptor by OEDocking. The plausible binding poses were scored by Chemgauss4 scoring function. Lastly, all the binding poses were visually inspected, from which the poses similar to that of novobiocin were retained for binding mode analysis.

ASSOCIATED CONTENT

AUTHOR INFORMATION

Corresponding Author

*E-mail: J.X. (jie.william.xia@hotmail.com) and S.W. (ws@imm.ac.cn)

Address: Jie Xia & Song Wu, Department of New Drug Research and Development, Institute of Materia Medica, Chinese Academy of Medical Sciences and Peking Union Medical College, Beijing 100050, China

ORCID

Wenjie Xue: 0000-0002-6621-6790

Jie Xia: 0000-0002-9567-3763

Hongmin Zhang: 0000-0003-4356-3615

Ya Chen: 0000-0001-5273-1815

Johannes Kirchmair: 0000-0003-2667-5877

Notes

The authors declare no competing financial interest.

Acknowledgements

This work was supported by the CAMS Innovation Fund for Medical Sciences (Grant No. 2017-I2M-1-012), the National Science and Technology Major Projects for Major New Drugs Innovation and Development (Grant No. 2018ZX09711001-012) and "Universities and Colleges Key Programs for Foreign Talent" of State Administration of Foreign Experts Affairs P.R. China (Grant No. T2018042). J.K. is supported by the Bergen Research Foundation (Grant No. BFS2017TMT01). Y.C. is supported by the China Scholarship Council (201606010345). We are grateful to OpenEye Scientific Software Inc. for providing their software with a Free Public Domain Research License.

Abbreviations

MRSA, methicillin-resistant *S. aureus*; VRE, vancomycin-resistant *E. faecium*; MIC, minimum inhibitory concentration; TFA, trifluroaceticacid; SAR, structure-activity relationship; MSSA, methicillin-sensitive S. aureus; MSSE, methicillin-sensitive S. epidermidis; MRSE, methicillin-resistant S. epidermidis; EFA, E. faecalis; EFM, E. faecium; VISA, vancomycin-intermediate S. aureus; HepG2, hepatocellular carcinoma; HUVEC, human umbilical vein endothelial cells; SRB, sulforhodamine B; SI, selectivity index; Cmax, maximum concentration; Tmax, time to reach the maximum concentration; MLD, minimum lethal dose; GyrB, DNA gyrase B; OD, optical density; MH, Mueller-Hinton; LU, luminescence.

References

[1] J. Xia, B. Feng, G. Wen, W. Xue, G. Ma, H. Zhang, S. Wu, Bacterial lipoprotein biosynthetic pathway as a potential target for structure-based design of antibacterial agents, Curr. Med. Chem., (2018).

[2] L.B. Rice, Federal funding for the study of antimicrobial resistance in nosocomial pathogens: no ESKAPE, The Journal of infectious diseases, 197 (2008) 1079-1081.

[3] H.W. Boucher, G.H. Talbot, J.S. Bradley, J.E. Edwards, D. Gilbert, L.B. Rice, M. Scheld, B. Spellberg, J. Bartlett, Bad bugs, no drugs: no ESKAPE! An update from the Infectious Diseases Society of America, Clinical infectious diseases : an official publication of the Infectious Diseases Society of America, 48 (2009) 1-12.

[4] U.C.f.D.C.a. Prevention, Antibiotic Resistance Threats in the United States. , in, https://www.cdc.gov/drugresistance/threat-report-2013/pdf/ar-threats-2013-508.pdf, 2013.

[5] D. Brown, Antibiotic resistance breakers: can repurposed drugs fill the antibiotic discovery void?, Nature Reviews Drug Discovery, 14 (2015) 821.

[6] E.D. Brown, G.D. Wright, Antibacterial drug discovery in the resistance era, Nature, 529 (2016) 336-343.

[7] J. Deng, L. Taheri, F. Grande, F. Aiello, A. Garofalo, N. Neamati, Discovery of novel anticancer compounds based on a quinoxalinehydrazine pharmacophore, ChemMedChem, 3 (2008) 1677-1686.

[8] G.A. Lemieux, J. Liu, N. Mayer, R.J. Bainton, K. Ashrafi, Z. Werb, A whole-organism screen identifies new regulators of fat storage, Nat. Chem. Biol., 7 (2011) 206-213.

[9] R. Dayam, T. Sanchez, N. Neamati, Discovery and structure-activity relationship studies of a unique class of HIV-1 integrase inhibitors, ChemMedChem, 1 (2006) 238-244.

[10] J.A. Maddry, S. Ananthan, R.C. Goldman, J.V. Hobrath, C.D. Kwong, C. Maddox, L. Rasmussen, R.C. Reynolds, J.A. Secrist, 3rd, M.I. Sosa, E.L. White, W. Zhang, Antituberculosis activity of the molecular libraries screening center network library, Tuberculosis, 89 (2009) 354-363.

[11] S. Ekins, A.C. Casey, D. Roberts, T. Parish, B.A. Bunin, Bayesian models for screening and TB Mobile for target inference with Mycobacterium tuberculosis, Tuberculosis, 94 (2014) 162-169.

[12] I.V.M. Ukrainets, E. V.; Sidorenko, L. V., 4-Hydroxy-2-quinolones. 122. 1-Hydroxy-3-oxo-5,6-dihydro-3H-pyrrolo[3,2,1- ij]-quinoline-2-carboxylic acid hetarylamides as potential antitubercular agents, Chem. Heterocycl. Compd., 43 (2007) 863.

[13] L. Peternel, M. Kotnik, A. Prezelj, U. Urleb, Comparison of 3 cytotoxicity screening assays and their application to the selection of novel antibacterial hits, J. Biomol. Screen., 14 (2009) 142-150.

[14] M. Ishankhodzhaeva, S.A. Kadyrova, M. Surazhskaya, N. Parpiev, P. Koz'min, Crystalline and Molecular Structure of 2-Amino-5-phenyl-1, 3, 4-thiadiazole, Russ. J. Org. Chem., 37 (2001) 721-723.

[15] H. Quan, H. Liu, C. Li, L. Lou, 1,4-Diamino-2,3-dicyano-1,4-bis(methylthio)butadiene (U0126) Enhances the Cytotoxicity of Combretastatin A4 Independently of Mitogen-Activated Protein Kinase Kinase, J. Pharmacol. Exp. Ther., 330 (2009) 326.

[16] Y. Niu, M. Wang, Y. Cao, A. Nimmagadda, J. Hu, Y. Wu, J. Cai, X.S. Ye, Rational Design of Dimeric Lysine N-Alkylamides as Potent and Broad-Spectrum Antibacterial Agents, J. Med. Chem., 61 (2018) 2865-2874.

[17] J. Hoque, M.M. Konai, S. Gonuguntla, G.B. Manjunath, S. Samaddar, V. Yarlagadda, J. Haldar, Membrane Active Small Molecules Show Selective Broad Spectrum Antibacterial Activity with No Detectable Resistance and Eradicate Biofilms, J. Med. Chem., 58 (2015) 5486-5500.

[18] V. Yarlagadda, P. Akkapeddi, G.B. Manjunath, J. Haldar, Membrane active vancomycin analogues: a strategy to combat bacterial resistance, J. Med. Chem., 57 (2014) 4558-4568.

[19] J.B. Houston, Utility of in vitro drug metabolism data in predicting in vivo metabolic clearance, Biochem. Pharmacol., 47 (1994) 1469-1479.

[20] C. Shi, Y. Zhang, T. Wang, W. Lu, S. Zhang, B. Guo, Q. Chen, C. Luo, X. Zhou, Y. Yang, Design, Synthesis, and Biological Evaluation of Novel DNA Gyrase-Inhibiting Spiropyrimidinetriones as Potent Antibiotics for Treatment of Infections Caused by Multidrug-Resistant Gram-Positive Bacteria, J. Med. Chem., 62 (2019) 2950-2973.

[21] V.J. Savage, C. Charrier, A.M. Salisbury, E. Moyo, H. Forward, N. Chaffer-Malam, R. Metzger, A. Huxley, R. Kirk, M. Uosis-Martin, G. Noonan, S. Mohmed, S.A. Best, A.J. Ratcliffe, N.R. Stokes, Biological profiling of novel tricyclic inhibitors of bacterial DNA gyrase and topoisomerase IV, J. Antimicrob. Chemother., 71 (2016) 1905-1913.

[22] D.A. Goff, J.E. Mangino, A.H. Glassman, D. Goff, P. Larsen, R. Scheetz, Review of Guidelines for Dental Antibiotic Prophylaxis for Prevention of Endocarditis and Prosthetic Joint Infections and Need for Dental Stewardship, Clin. Infect. Dis., (2019).

[23] T. Lehrnbecher, B.T. Fisher, B. Phillips, S. Alexander, R.A. Ammann, M. Beauchemin, F. Carlesse, E. Castagnola, B.L. Davis, L.L. Dupuis, G. Egan, A.H. Groll, G.M. Haeusler, M. Santolaya, W.J. Steinbach, M. van de Wetering, J. Wolf, S. Cabral, P.D. Robinson, L. Sung, Guideline for Antibacterial Prophylaxis Administration in Pediatric Cancer and Hematopoietic Stem Cell Transplantation, Clin. Infect. Dis., (2019).

[24] S. Schmidt, D. Gonzalez, H. Derendorf, Significance of Protein Binding in Pharmacokinetics and Pharmacodynamics, J. Pharm. Sci., 99 (2010) 1107-1122.

[25] M. Schechner, F. Sirockin, R.H. Stote, A.P. Dejaegere, Functionality maps of the ATP binding site of DNA gyrase B: generation of a consensus model of ligand binding, J. Med. Chem., 47 (2004) 4373-4390.

[26] J.M. May, T.W. Owens, M.D. Mandler, B.W. Simpson, M.B. Lazarus, D.J. Sherman, R.M. Davis, S. Okuda, W. Massefski, N. Ruiz, D. Kahne, The Antibiotic Novobiocin Binds and Activates the ATPase That Powers Lipopolysaccharide Transport, J. Am. Chem. Soc., 139 (2017) 17221-17224.

[27] N. Zidar, T. Tomasic, H. Macut, A. Sirc, M. Brvar, S. Montalvao, P. Tammela, J. Ilas, D. Kikelj, New N-phenyl-4,5-dibromopyrrolamides and N-Phenylindolamides as ATPase inhibitors of DNA gyrase, Eur. J. Med. Chem., 117 (2016) 197-211.

[28] M. Davies, M. Nowotka, G. Papadatos, N. Dedman, A. Gaulton, F. Atkinson, L. Bellis, J.P. Overington, ChEMBL web services: streamlining access to drug discovery data and utilities, Nucleic Acids Res., 43 (2015) W612-W620.

[29] A. Gaulton, A. Hersey, M. Nowotka, A.P. Bento, J. Chambers, D. Mendez, P. Mutowo, F. Atkinson, L.J. Bellis, E. Cibrián-Uhalte, M. Davies, N. Dedman, A. Karlsson, M.P. Magariños, J.P. Overington, G. Papadatos, I. Smit, A.R. Leach, The ChEMBL database in 2017, Nucleic Acids Res., 45 (2017) D945-D954.

[30] J.B. Cross, J. Zhang, Q. Yang, M.F. Mesleh, J.A. Romero, B. Wang, D. Bevan, K.M. Poutsiaka, F. Epie, T. Moy, A. Daniel, J. Shotwell, B. Chamberlain, N. Carter, O. Andersen, J. Barker, M.D. Ryan, C.A. Metcalf, 3rd, J. Silverman, K. Nguyen, B. Lippa, R.E. Dolle, Discovery of Pyrazolopyridones as a Novel Class of Gyrase B Inhibitors Using Structure Guided Design, ACS Med. Chem. Lett., 7 (2016) 374-378.

[31] R.R. Kale, M.G. Kale, D. Waterson, A. Raichurkar, S.P. Hameed, M.R. Manjunatha, B.K. Kishore Reddy, K. Malolanarasimhan, V. Shinde, K. Koushik, L.K. Jena, S. Menasinakai, V. Humnabadkar, P. Madhavapeddi, H. Basavarajappa, S. Sharma, R. Nandishaiah, K.N. Mahesh Kumar, S. Ganguly, V. Ahuja, S. Gaonkar, C.N. Naveen Kumar, D. Ogg, P.A. Boriack-Sjodin, V.K. Sambandamurthy, S.M. de Sousa, S.R. Ghorpade, Thiazolopyridone ureas as DNA gyrase B inhibitors: optimization of antitubercular activity and efficacy, Bioorg. Med. Chem. Lett., 24 (2014) 870-879.

[32] S. Alt, L.A. Mitchenall, A. Maxwell, L. Heide, Inhibition of DNA gyrase and DNA topoisomerase IV of Staphylococcus aureus and Escherichia coli by aminocoumarin antibiotics, J. Antimicrob. Chemother., 66 (2011) 2061-2069.

[33] J. Zhang, Q. Yang, J.B. Cross, J.A. Romero, K.M. Poutsiaka, F. Epie, D. Bevan, B. Wang, Y. Zhang, A. Chavan, X. Zhang, T. Moy, A. Daniel, K. Nguyen, B. Chamberlain, N. Carter, J. Shotwell, J. Silverman, C.A. Metcalf, 3rd, D. Ryan, B. Lippa, R.E. Dolle, Discovery of Azaindole Ureas as a Novel Class of Bacterial Gyrase B Inhibitors, J. Med. Chem., 58 (2015) 8503-8512.

[34] E. Martens, A.L. Demain, The antibiotic resistance crisis, with a focus on the United States, J. Antibiot., 70 (2017) 520-526.

[35] I. Ukrainets, L. Yangyang, A. Tkach, O. Gorokhova, A. Turov, 4-hydroxy-2-quinolones 165*. 1-R-4-hydroxy-2-oxo-1, 2-dihydro-quinoline-3-carbaldehydes and their thiosemicarbazones. Synthesis, structure, and biological properties, Chem. Heterocycl. Compd., 45 (2009) 705.

[36] G.M. Coppola, G.E. Hardtmann, The chemistry of 2H-3,1-benzoxazine-2,4(1H)dione (isatoic anhydride). 7. Reactions with anions of active methylenes to form quinolines, J. Heterocycl. Chem., 16 (1979) 1605-1610.

[37] M.A. Wikler, Methods for dilution antimicrobial susceptibility tests for bacteria that grow aerobically : approved standard, Clinical and Laboratory Standards Institute, 26 (2006) M7-A7.

[38] C.I. Bliss, The Calculation of the dosage-mortality curve, Ann. Appl. Biol., 22 (1935) 134-167.

[39] P.C. Hawkins, A.G. Skillman, G.L. Warren, B.A. Ellingson, M.T. Stahl, Conformer generation with OMEGA: algorithm and validation using high quality structures from the

Protein Databank and Cambridge Structural Database, J. Chem. Inf. Model., 50 (2010) 572-584.

[40] M. McGann, FRED pose prediction and virtual screening accuracy, J. Chem. Inf. Model., 51 (2011) 578-596.

- Medicinal chemistry efforts lead to a novel antibacterial agent g37.
- No evidence of resistance development was observed for g37.
- g37 is orally active to treat MRSA infection.
- g37 inhibits the ATPase activity of Gyrase B and impairs *S. aureus* DNA supercoiling.
- g37 can be further developed into a new class of antibacterial agents.

Declaration of Interest Statement

The authors declare no competing financial interest.